HORIZONTAL STIFFNESS & DAMPING OF PILES IN INHOMOGENEOUS SOIL

Xenia KARATZIA[1] and George MYLONAKIS[2]

Abstract: A practically-oriented analytical procedure for determining the dynamic stiffness and damping (impedance coefficients) of a laterally-loaded pile in soil exhibiting different types of inhomogeneity with depth, is presented. To this end, an energy method based on the Winkler model of soil reaction in conjunction with pertinent shape functions for the deflected shape of the pile, are employed. A new elastodynamic model for the wave field around a pile is also introduced. The method is self-standing and free of empirical formulae or constants. Dimensionless closed-form solutions are derived for: (1) the distributed (Winkler) springs and dashpots along the pile; (2) the dynamic stiffness and damping coefficients at the pile head; (3) the "active" length beyond which the pile can be treated as infinitely long; (4) the relative contributions to the overall head stiffness and damping of the soil and the pile media. Swaying, rocking and cross swaying-rocking impedances are considered for parabolic, exponential, and multi-layered inhomogeneous soil. The predictions of the model compare favorably with established solutions, while new results are presented. An illustrative example is provided.

Keywords: *pile, stiffness, damping, closed-form solution, soil-structure interaction, radiation damping.*

[1]Ph.D. Candidate, Dept. of Civil Engineering, Univ. of Patras, Rio 26500, Greece. Email: kseniakaratzia@yahoo.gr

[2]Professor, Dept. of Civil Engineering, Univ. of Bristol, Queens Building, Bristol BS8 1TR, U.K.; Professor, Dept. of Civil Engineering, Univ. of Patras, Rio 26500, Greece; Adjunct Professor, Univ. of California at Los Angeles, CA 90095 (corresponding author). E-mail: mylo@upatras.gr, g.mylonakis@bristol.ac.uk

INTRODUCTION

Systematic research over the past decades on the dynamics of laterally-loaded piles has resulted in a wide set of analysis methods that can be used in design. These methods can be classified in two broad groups: 1) those based on the beam-on-Winkler-foundation model, and 2) those based on the continuum model. Reviews of the subject have been presented, among others, by Pender (1993) and Gazetas & Mylonakis (1998).

With reference to the first group of methods, the assumption of an Euler-Bernoulli beam for the pile is usually valid, since most piles are sufficiently slender so that shear deformations in their body can be neglected. On the other hand, the representation of the restraining action of soil via independent springs distributed along the pile axis is not straightforward, since the spring modulus cannot be determined by elementary means ignoring soil-structure interaction such as borehole data (Mylonakis 2001; Basu & Salgado 2008; Guo 2012). Moreover, the common assumption of uniform soil stiffness is usually unrealistic, as overburden stresses combined with over-consolidation and stress-induced nonlinearities due to pile installation and subsequent loading typically result in soil stiffness varying with depth. Due to inherent difficulties in handling variable material properties analytically, there is a lack of solutions for the response of piles in inhomogeneous soil (Syngros 2004; Basu & Salgado 2008; Guo 2012). Indeed, exact analytical solutions obtained by means of Winkler models are restricted to the idealized case where soil modulus increases proportionally with depth i.e., a triangular distribution, and static conditions (Hetenyi 1946). These solutions are expressed in terms of infinite power series, which are hard to implement in practice. Analytical solutions for dynamic loads based on more rigorous methods are not available.

A variant of the subgrade reaction method is the *p-y* method, which is widely employed in the offshore industry for large amplitude static or low-frequency loads (Guo 2012). Extending the method to dynamic conditions is not straightforward given the theoretical difficulties in

handling non-linear dynamic effects and the scarcity of experimental data (Gerber & Rollins, 2008). Another drawback of this approach is the site-specific nature experimentally obtained *p-y* curves which do not fully respect the three-dimensional aspects of pile-soil interaction (Basu & Salgado, 2008).

With reference to the second group of methods, numerical solutions to the problem have been published, among others, by Banerjee & Davies (1978), Kulhemeyer (1979), Poulos & Davis (1980), Randolph (1981), Kaynia & Kausel (1982), Budhu & Davis (1987) and El-Marsafawi et al (1992) using a variety of analytical techniques including finite-difference, finite-element, boundary-element and various hybrid formulations in three dimensions. These methods are mathematically involved and, thereby, not appealing to geotechnical engineers. With the exception of a few fitted formulas pertaining to linearly- and parabolically-varying stiffness with depth (Randolph 1981; Budhu & Davis 1987; Gazetas 1991; Syngros 2004), little information is available about pile stiffness and damping in inhomogeneous soil media.

The aim of this paper is to develop a theoretically sound, yet practically-oriented analysis procedure for determining the dynamic stiffness and damping of flexible laterally-loaded piles considering more general types of soil inhomogeneity. To this end, the following novel solutions are presented and discussed:

(1) a 2D elastodynamic model for the modulus of the distributed dashpots along the pile,

(2) a 3D elasticity solution for the modulus of the distributed springs,

(3) an energy method for the stiffness and damping coefficients at the pile head.

The method allows for closed-form solutions to be obtained for a variety of soil profiles, including a multi-layer one which can handle any type of vertical inhomogeneity. Unlike existing approximate methods employing fitted formulas to finite-element solutions, the procedure is self-standing and does not involve empirical information. Moreover, the method

77 can be extended to model, in an iterative manner, nonlinear problems via pertinent *p-y*
78 relations – although such applications are not examined here (Gerolymos & Gazetas, 2005b).
79 The problem investigated is depicted in Fig. 1a: a laterally-loaded pile embedded in a soil
80 profile whose stiffness varies with depth, loaded by a concentrated force and/or a moment at
81 the head. The pile is considered a linearly visco-elastic solid cylindrical beam of diameter d,
82 Young's modulus E_p and linear hysteretic damping β_p. It is also assumed that the pile is
83 sufficiently long so that it deforms only up to a certain depth, L_a – known in the literature as
84 "active length", which is typically on the order of ten pile diameters (Kulhemeyer 1979;
85 Randolph 1981). The soil is modeled as a linearly viscoelastic medium of Young's modulus
86 E_s, Poisson's ratio ν, mass density ρ_s, and linear hysteretic damping β_s.
87
88 **SOIL DESCRIPTION**
89 Fig. 2 depicts three basic forms of soil stiffness variation with depth considered in this work:
90 a) a "generalized parabolic" profile in which soil Young's modulus increases with depth
91 according to a power law, starting from a finite value at the surface; b) a profile in which soil
92 stiffness varies exponentially between two finite values at zero and infinite depth,
93 respectively – to be referred in the ensuing to as an "exponential" profile, and c) a multi-layer
94 profile with each horizontal layer having arbitrary thickness and material properties.
95 Of these soil conditions, the third and certain special cases of the first (e.g. the case where
96 stiffness increases proportionally with depth) are the ones adopted in most of the literature.
97 The second profile has been first treated, for a different class of geotechnical problems, by
98 Selvadurai et al. (1986) and Vrettos (1991).
99 The generalized parabolic variation of soil Young's modulus with depth depicted in Fig. 2a is
100 described by the equation
101 $$E_s(z) = E_{sd}\left[a + (1-a)\,z/d\right]^n \qquad (1)$$

where E_{sd} denotes soil Young's modulus at depth of one pile diameter ($z=d$), while a and n are dimensionless inhomogeneity parameters.

Setting $z = 0$ in Eq. (1), a is obtained as

$$a = \left(E_{s0}/E_{sd}\right)^{1/n} \tag{2}$$

where E_{s0} stands for the soil Young's modulus at the surface. The exponent n typically varies between zero and one, corresponding to over-consolidated and normally consolidated clay, respectively. A value of one half pertains to uncemented granular soil such as sand (Darendeli 2001; Muir Wood 2004).

With reference to the modulus of the Winkler springs, it is postulated that $k(z)$ follows the same variation with depth as $E_s(z)$ i.e.,

$$k\left(z\right) = k_d\left[a + \left(1-a\right)z/d\right]^n \tag{3}$$

where k_d denotes the value of the spring constant at the depth of one pile diameter.

Both k_d and E_{sd} are measured in units of pressure and are related through

$$k_d = \delta E_{sd} \tag{4}$$

δ being a dimensionless coefficient typically varying between 1 to 2 depending on variation of soil stiffness with depth, pile-soil stiffness contrast and boundary conditions at the pile head (Novak et al 1978; Roesset 1980; Scott 1981; Dobry et al 1982; Gazetas & Dobry 1984; Syngros 2004; Karatzia et al 2014).

With reference to radiation damping, it is known from dimensional considerations (Kuhlemeyer 1979) that the dashpot coefficient c_r is proportional to soil shear wave velocity V_s (i.e., $\sqrt{E_s}$). Accordingly, as a first approximation, one may write

$$c_r(z) = c_{rd}\left[a + \left(1-a\right)z/d\right]^{n/2} \tag{5}$$

which reveals a weaker dependence of c_r on depth compared to k in Eq. (3). In the above equation c_{rd} stands for the dashpot modulus at $z = d$. Frequency effects on radiation damping are discussed later in this article.

Bounded soil inhomogeneity with depth, depicted in Fig. 2b, can be taken into account by considering an exponential variation in Young's modulus with depth of the form (Vrettos 1991)

$$E_s(z) = E_{s\infty}\left[b + (1-b)\left(1 - e^{-qz/d}\right)\right] \tag{6}$$

in which b stands for the ratio of Young's moduli at the surface (E_{s0}) and at infinite depth ($E_{s\infty}$), while q is a dimensionless inhomogeneity parameter controlling the rate of increase or decrease in stiffness.

In the same vein as in Eqs (3) and (5), the moduli of the Winkler springs and dashpots for the case of bounded soil inhomogeneity can be written as

$$k(z) = k_d \frac{b + (1-b)\left(1 - e^{-qz/d}\right)}{b + (1-b)\left(1 - e^{-q}\right)} \quad , \quad c_r(z) = c_{rd}\left[\frac{b + (1-b)\left(1 - e^{-qz/d}\right)}{b + (1-b)\left(1 - e^{-q}\right)}\right]^{1/2} \tag{7a,b}$$

with k_d and c_{rd} having the same meaning as before.

Bounded inhomogeneity such as that expressed by Eqs (6) and (7) might be preferable over the unbounded one in Eqs (1) to (5) for deep soil profiles. However, for shallower profiles either form may be suitable and the selection should be made on a case by case basis.

RADIATION DAMPING MODEL

Several simplified models based on different assumptions regarding wave propagation in the soil have been proposed for evaluating the distributed radiation dashpot coefficient along the pile. Fig. 3 illustrates a number of radiation damping schemes. A brief reference to these mechanisms is useful and reveals salient features of the proposed analysis.

147 The stripe model of Berger et al (1977) assumes 1D wave propagation in an infinitely long
148 constrained rod and a viscous dashpot which fully absorbs the energy of the emitting waves.
149 Despite its simplicity, this model lacks realism because it provides a strictly frequency-
150 independent c_r with high sensitivity to Poisson's ratio, producing an infinite amount of
151 damping as v approaches 0.5. A more rigorous approach has been followed by Novak et al
152 (1978), who proposed a 2D plane-strain model. In this idealization, the soil is divided into an
153 infinite number of thin horizontal "slices", with each slice subjected to dynamic plane-strain
154 deformation (i.e., $\varepsilon_z = 0$). The resulting radiation damping coefficient is frequency-dependent
155 and decreases monotonically with frequency. The validity of this model has been
156 demonstrated in the works of Blaney et al (1976) and Roesset (1980).
157 An alternative plane-strain scheme has been developed by Gazetas & Dobry (1984). The
158 basic assumption is that the circular cross section of the foundation can be approximated by a
159 square cross section and the surrounding soil is divided into four trapezoidal zones. This
160 formulation allows each of the zones to be analyzed separately as a two-dimensional
161 truncated cone, with compression and extension taking place along the direction of the
162 imposed load and pure shear developing in the perpendicular direction. Based on this
163 formulation, the authors derived an approximate, frequency dependent radiation damping
164 coefficient $c_r/(d\pi\rho_s V_s) = [1/(2\pi)]^{1/4}[1+(V_s/V_c)^{-5/4}]a_0^{-1/4}$, with a_0 ($= \omega d/V_s$) being the familiar
165 dimensionless frequency, ω being the cyclic excitation frequency and V_c standing for the
166 compressional wave propagation velocity in the soil, which was empirically set equal to the
167 so-called Lysmer's analog wave velocity V_{La} $(= 3.4V_s / [\pi(1-v)])$.
168 An alternative plane-strain model, henceforward referred to as an "infinitesimal sector
169 model", is illustrated in Fig. 3d. Contrary to the earlier formulation, in the present model the
170 soil is divided into an infinite number of thin independent sectors, with each sector
171 responding to dynamic compression and shearing independent of the others. Under this

physically-motivated assumption the circular cross section does not need to be replaced by a rectangular one. It is further assumed that each of the independent infinitesimal sectors emits shear and compressional waves, considering that in the loading direction and the perpendicular one propagate only compressional and shear waves, respectively. Shear waves are assumed to propagate with velocity V_s, while compression waves propagate with velocity V_c. As shown in the Supplemental Data File, each sector possesses an infinitesimal amount of stiffness expressed in the global reference system as a function of the polar angle ϕ defined in Fig. 3d and the dimensionless frequency a_0.

By integrating the contributions of all sectors, it is easy to show that the spring and the radiation damping coefficient in an undamped soil medium are, respectively

$$\frac{k}{G_s} = \pi a_0 \frac{1}{2}\mathrm{Re}[\Lambda] \quad , \quad \frac{c_r}{d\pi\rho_s V_s} = \frac{1}{2}\mathrm{Im}[\Lambda] \tag{8a,b}$$

where,

$$\Lambda = \left(\frac{V_s}{V_c}\right)^{-1} \frac{H_1^{(2)}\left(\frac{1}{2}\frac{V_s}{V_c}a_0\right)}{H_0^{(2)}\left(\frac{1}{2}\frac{V_s}{V_c}a_0\right)} + \frac{H_1^{(2)}\left(\frac{1}{2}a_0\right)}{H_0^{(2)}\left(\frac{1}{2}a_0\right)} \tag{9}$$

is a dimensionless function of frequency, $H_0^{(2)}$ and $H_1^{(2)}$ being, respectively, the zero- and first-order Hankel functions of the second kind.

The relationship in Eqs (8b) and (9) is identical to that of Gazetas & Dobry (1984), except for the generic velocity ratio (V_s/V_c) – instead of an empirically defined compression velocity of the earlier model – and the absence of a multiplier $\pi/4$, which reflects the ratio of the side length to the diameter of a square pile cross section and a circular one, respectively, of equal perimeters. Evidently, these differences do not affect the functional form of the solution, yet may have an appreciable impact on the numerical results, as demonstrated in the following.

It should be noticed that contrary to the aforementioned models, the horizontal soil slices are considered here to be semi-restricted (i.e., it is assumed that the vertical dynamic stress

195 increment σ_z is zero, instead of the corresponding shear strain ε_z), a superior approximation
196 accounting for the effect of the free surface and leading to solutions not strongly dependent
197 on Poisson's ratio, in agreement with rigorous numerical solutions of related problems
198 (Veletsos & Younan 1995; Anoyatis & Mylonakis 2012). In light of this assumption, V_s/V_c =
199 $[(1-\nu)/2]^{1/2}$. A detailed discussion of this equation is provided in Anoyatis et al (2016).
200 A comparison of the predictions of the proposed model against those available in the
201 literature is provided in Fig. 4a for the cases where ν = 0.25 and 0.4. Evidently, there is good
202 agreement between the four solutions. The Tabesh & Poulos (2000) proposal of $c_r = 5dp_sV_s$
203 seems to provide a reasonable approximation for dimensionless frequencies a_0 on the order of
204 1. At higher frequencies it can be shown that Λ approaches asymptotically the purely
205 imaginary value $i[1+(V_s/V_c)^{-1}]$ and, thereby, the radiation dashpot c_r becomes frequency
206 independent while the spring constant vanishes, as in the one dimensional case.
207 Using non-linear regression analysis by means of the Levenberg-Marquardt method
208 (Bevington and Robinson 1992) in the results of Fig. 4b in the frequency range $0.1 < a_0 < 1$,
209 the following predictive equation is derived

210 $$\frac{c_r}{d\pi\rho_s V_s} = \left[0.25 + 0.8\left(\frac{V_s}{V_c}\right)^{-1}\right] a_0^{-0.4} \qquad (10)$$

211 which can be used in applications. It must be noted that the infinitesimal sector model also
212 provides information on Winkler spring stiffness (Eq. 8a). However, the stiffness tends to
213 zero both at low and high frequencies and, thereby, the solution is of limited value. An
214 enhanced stiffness model is presented later in this article.
215

216 **PILE STIFFNESS MODEL**

217 Under harmonic oscillations, the equation of motion of a uniform pile attached to a Winkler
218 foundation with variable modulus $k(z)$ and $c_r(z)$, is (Mylonakis 1995)

$$E_p I_p \frac{d^4 Y}{dz^4} + \left[k(z) - m\omega^2 + i\omega c_r(z) \right] Y = 0 \qquad (11)$$

where $Y = Y(z)\ exp[i\ \omega t]$ is the harmonic pile deflection as a function of depth z; E_pI_p is the pile flexural stiffness, m is the pile mass per unit length, $k(z)$ and $c_r(z)$ are the moduli of Winkler springs and dashpots, ω being the cyclic excitation frequency and $i = \sqrt{-1}$.

In case of a homogeneous soil layer, solving Eq. (11) is straightforward. The associated impedance coefficients in swaying, rocking and cross swaying-rocking are, respectively (Scott 1981; Dobry et al 1982; Pender 1993; Mylonakis 1995)

$$K_{hh} = 4E_p I_p \lambda^3, \quad K_{rr} = 2E_p I_p \lambda, \quad K_{hr} = 2E_p I_p \lambda^2 \qquad (12a\text{-}c)$$

where

$$\lambda = \left[\frac{k + i\omega c_r - m\omega^2}{4E_p I_p} \right]^{1/4} \qquad (13)$$

is a Winkler parameter, measured in units of 1/Length, which can be interpreted as a wavenumber controlling the attenuation of pile deflection with depth.

The basis of the proposed solution is that the unknown deflection function $Y(z)$ in Eq. (11) can be effectively represented by a pair of approximate, twice differentiable, dimensionless unitary functions $\chi(z)$ and $\varphi(z)$ (Fig. 1). Of these functions, $\chi(z)$ represents the normalized deflected shape of the pile due to a unit head displacement under zero rotation (Fig. 1b), whereas $\varphi(z)$ is the corresponding deflected shape due to a unit head rotation under zero displacement (Fig. 1c). For long piles, $\chi(z)$ and $\varphi(z)$ can be well approximated by the deflected shape of a long pile in homogeneous soil (Karatzia & Mylonakis 2012):

$$\chi(z) = e^{-\mu z}\left[\sin(\mu z) + \cos(\mu z) \right], \qquad \varphi(z) = \frac{e^{-\mu z}}{\mu} \sin(\mu z) \qquad (14a,b)$$

For a free-head pile loaded by a horizontal head force, the corresponding function is (Fig. 1d)

$$\psi(z) = e^{-\mu z} \cos(\mu z) \qquad (14c)$$

In the above equations μ is a shape parameter analogous to the wavenumber λ in Eq. (13). In homogeneous soil λ and μ coincide. In non-homogeneous soil μ can be taken as the mean value of λ within the active length, L_a, of the pile i.e.,

$$\mu = \frac{1}{L_a}\int_0^{L_a} \lambda(z,\omega)\,dz \tag{15}$$

It should be noticed that L_a is defined as the length beyond which the pile behaves as a semi-infinite beam that is, an increase in pile length would lead to an asymptotic change (increase or decrease) in lateral stiffness at the pile head, regardless of boundary conditions at the tip. Pertinent expressions for L_a in various soil profiles are derived in the following.

Replacing $Y(z)$ in Eq. (11) with $Y_o\,\chi_i(z)$, Y_o being the amplitude of motion at the pile head, multiplying by $Y_o\,\chi_j(z)$, χ_i, χ_j being any of the shape functions in Eqs (14a) and (14b), and integrating over the length of the pile, it can be easily shown (Mylonakis & Roumbas 2001; Karatzia & Mylonakis 2012) that the stiffness and damping coefficients atop the pile can be determined from the virtual-work equations

$$K_{ij} = E_p I_p \int_0^L \chi_i''(z)\,\chi_j''(z)\,dz + \int_0^L k(z)\chi_i(z)\,\chi_j(z)\,dz - m\omega^2\int_0^L \chi_i(z)\,\chi_j(z)\,dz \tag{16a}$$

$$C_{ij} = \frac{2\beta_p E_p I_p}{\omega}\int_0^L \chi_i''(z)\,\chi_j''(z)\,dz + \frac{2\beta_s}{\omega}\int_0^L k(z)\chi_i(z)\,\chi_j(z)\,dz + \int_0^L c_r(z)\chi_i(z)\,\chi_j(z)\,dz \tag{16b}$$

which are analogous to energy approximations used in finite-element procedures (Clough & Penzien 1975; Mylonakis 1995). Note that the first two terms in the right-hand side of Eq. (16a) stand for the contribution to the overall stiffness of pile flexural stiffness and soil stiffness, respectively. The contribution of pile inertia to stiffness (third term in Eq. 16a) is typically minor and, thereby, is omitted in the remainder of this work. Accordingly, pile head stiffness can be well approximated by its static value in the frequency range of interest in earthquake engineering applications (Kaynia & Kausel 1982).

In Eq. (16b), the first two terms stand for the contributions to overall damping of the pile and the soil material damping, respectively, while the last term corresponds to the contribution of

soil radiation damping. The method was first employed in the analysis of pile foundations by Dobry et al (1982) and later by Gazetas & Dobry (1984), who determined the swaying damping coefficient C_{hh} using Eq. (16b) in conjunction with a numerically-evaluated shape function for a fixed-head pile.

The subscripts i and j in the above formulation refer to different vibrational modes (i.e., swaying and rocking). For instance, using $\chi_i(z) = \chi_j(z) = \chi(z)$ the swaying impedance coefficients K_{hh} and C_{hh} are obtained. Similarly, setting $\chi_i(z) = \chi_j(z) = \varphi(z)$, Eqs (16a,b) yield the rocking impedance coefficients K_{rr} and C_{rr}. Finally, using $\chi_i(z) = \chi(z)$ and $\chi_j(z) = \varphi(z)$ generates the cross swaying-rocking impedances K_{hr} and C_{hr}. It is implicitly assumed that $\chi(z)$ and $\varphi(z)$ are real-valued, obtained by static considerations. Also, for $L > L_a$ the analysis can be simplified by considering the pile as infinitely long, thereby increasing the upper integration limit in Eqs. (16a,b) to infinity. These approximations have been established in earlier studies by Dobry et al (1982), Mylonakis (1995) and Mylonakis & Gazetas (1999).

To develop insight into the physics of the solution, it is useful to adopt a representation of pile head stiffness in the form

$$K_{ij} = K_{ij}^{p}\left(1 + S_{ij}\right) \tag{17}$$

where K^{p}_{ij} denotes the contribution to the overall head stiffness of pile flexural stiffness (first integral in Eq. 16a) and S_{ij} is a dimensionless coefficient which stands for the contribution of the restraining action of soil (second integral in Eq. 16a normalized by the first). Accordingly,

$$K_{hh} = E_p I_p \mu^3 \left(1 + S_{hh}\right) \quad , \quad K_{rr} = \frac{3}{2} E_p I_p \mu \left(1 + S_{rr}\right) \quad , \quad K_{hr} = E_p I_p \mu^2 \left(1 + S_{hr}\right) \tag{18a-c}$$

which correspond to the swaying, rocking and cross-swaying-rocking mode, respectively. For homogeneous soil the coefficients S_{ij} equal 3, 1/3 and 1, respectively, according to Eq. (12).

In addition, using the normalized damping coefficient at the pile head

289 $$\beta_{ij} = \frac{\omega C_{ij}}{2K_{ij}} \quad (19)$$

290 Eq. (16b) yields the dimensionless expression

291 $$\beta_{ij} = w_{ij}^{p}\,\beta_{p} + \left(1 - w_{ij}^{p}\right)\beta_{s} + w_{ij}^{r}\,\beta_{rd} \quad (20)$$

292 where w^{p}_{ij}, w^{r}_{ij} are dimensionless coefficients which stand for the contribution to the overall
293 damping of pile material damping and radiation damping, respectively. These coefficients are
294 dependent on the response mode, type of soil inhomogeneity and E_p/E_{sd} ratio.
295 The distributed radiation damping coefficient along the pile, β_{rd}, is

296 $$\beta_{rd} = \frac{\omega\, c_{rd}}{2\, k_{d}} \quad (21)$$

297 c_{rd} being the value of the radiation dashpot at $z = d$.
298 In the realm of the proposed elastodynamic model, $\beta_{rd} = \pi\ Im[\Lambda]\ a_{0d} / [8(1+\nu)\ \delta]$ (following
299 Eqs. 4, 8b), a_{0d} being the dimensionless frequency at depth $z = d$ (i.e., $\omega d / V_{sd}$).
300 By matching Eqs. (20) and (16b), the weight factors w^{p}_{ij} are related to S_{ij} in Eq. (17) through

301 $$w_{ij}^{p} = \frac{1}{1 + S_{ij}} \quad (22)$$

302 which suggests that the dimensionless coefficients S_{ij} and w^{r}_{ij} (six factors in total) suffice to
303 describe the dynamic impedance of a cylindrical pile in planar oscillations.
304

305 ## WINKLER SPRING STIFFNESS MODEL

306 Key to the implementation of the proposed method is the appropriate selection of the Winkler
307 spring coefficient δ in Eq. (4). This can be done based on a three-dimensional elasticity
308 model for the response of a horizontal soil slice proposed by the senior author (Mylonakis
309 2001). The difference with the slice model in Fig. 3d lies in the horizontal inter-slice shear
310 tractions at the upper and lower faces of the slice which are accounted for, providing finite

311 stiffness at all frequencies. The above solution (which contains some clerical errors in the
312 original publication), is further explained in Karatzia et al (2014, 2015) and can be cast as

313 $$\delta = \frac{2\pi\eta_u^2}{(1+\nu)}\left\{\ln\left[\eta_u\left(4/a_c\right)^{1+\eta_u^2}\right]-\gamma\left(1+\eta_u^2\right)\right\}^{-1} \quad (23)$$

314 where $\eta_u=[(2-\nu)/(1-\nu)]^{1/2}$ is a compressibility coefficient, γ (= 0.577) is Euler's number, and
315 α_c is a dimensionless parameter accounting for the variation of pile displacement with depth

316 $$\alpha_c = d\left(\int_0^\infty G_s(z)Y'(z)^2\,dz \Big/ \int_0^\infty G_s(z)Y(z)^2\,dz\right)^{1/2} \quad (24)$$

317 where $Y = Y(z)$ is the deflected shape of the pile in Eq. (11) (Eqs 14a-c for various response
318 modes) and $G_s(z)$ [= E_s(z) / 2(1+ν)] is the depth-varying soil shear modulus.
319 Evaluating Eq. (24) yields

320 $$\alpha_c = \chi_\delta\left(E_p/E_{sd}\right)^{n_\delta} \quad (25)$$

321 with χ_δ and n_δ given in Table 1 for different soil profiles and pile head constraints. It is worth
322 noting that in a shallow soil layer over a rigid base, parameter α_c can be interpreted as a
323 cutoff frequency beyond which propagating waves suddenly emerge in the soil. However, for
324 the more general conditions at hand, α_c can be viewed as a stiffness parameter.
325 A comparison of the predictions of Eq. (23) against available formulas for parameter δ is
326 performed graphically in Fig. 5, with reference to fixed- and free-head piles in homogeneous
327 soil. Evidently, the effect of pile head restraint is significant and becomes more pronounced
328 at low pile-soil stiffness contrasts. The proposed model captures satisfactorily this effect. In
329 general, parameter δ is on the order of 1 and 2 for both fixed- and free-head piles, and tends
330 to decrease with increasing E_p/E_s. The proposed analytical solution is in good agreement with
331 the available formulae, especially for stiff piles having E_p/E_s ratios greater than 10^3 or so.
332 Fig. 6 presents results for parameter δ in different soil profiles obtained with the proposed
333 model. Clearly, δ is sensitive to the type of soil profile attaining greater values in soil whose
334 stiffness varies with depth. This is hardly surprising as the gradient of Young's modulus with

depth increases the interaction ("arching") among soil slices at different elevations. With reference to the fixity condition at the pile head, parameter δ is much higher for free-head piles in the whole range of E_p/E_{sd} values. A comparison of the present solution against results from the finite-element-based solution of Syngros (2004) is presented in the same graph. The accord between the proposed method and the numerical solution cannot be overstated especially for piles with E_p/E_{sd} ratios greater than 10^3 or so.

ACTIVE PILE LENGTH

It is well-known that the response of a laterally-loaded pile becomes essentially independent of pile length after a critical limit known as "active length", L_a. Several empirical formulae have been proposed to estimate this parameter (Kuhlmeyer 1979; Poulos & Davis, 1980; Randolph 1981; Fleming et al 1993; Gazetas 1991; Budhu & Davies 1987; Mylonakis 1995; Syngros 2004; Guo 2012; Di Laora & Rovithis 2015). These are typically written in the form

$$L_a/d = \chi_L \left(E_p/E_{sd}\right)^{n_L} \tag{26}$$

χ_L and n_L being dimensionless constants; n_L is of the order of 0.25 while χ_L lies in the range 1.5 to 2.5 depending mainly on type of soil profile and fixity conditions at pile head.

In the realm of the present model, a rational estimation of active pile length is possible by means of simple calculations. The investigation at hand focuses on both homogeneous and inhomogeneous soil. Based on Eq. (16a) and the developments of the previous sections, the following dimensionless equation is derived for the stiffness coefficient K_{hh}

$$\varepsilon_{tol} = \frac{E_p I_p \int_{L_a}^{\infty} \chi''(z)^2 \, dz + \int_{L_a}^{\infty} k(z) \chi(z)^2 \, dz}{E_p I_p \mu^3 + \int_0^{\infty} k(z) \chi(z)^2 \, dz} \tag{27}$$

in which $\chi(z)$ is the shape function in Eq. (14a) and ε_{tol} stands for a tolerance parameter. In the above ratio, the denominator represents the stiffness coefficient K_{hh} of an infinitely long pile whereas the numerator stands for the contribution of the portion of the pile below the active

length. Accordingly, a value of ε_{tol} equal to 10^{-2} suggests that 99% of the swaying stiffness K_{hh} is contributed by the portion of the pile above L_a. Based on existing literature (Randolph 1981; Syngros 2004), ε_{tol} is usually taken in the range 10^{-2} to 10^{-3}. Note that the formulation in Eq. (27) is general and can be applied to both homogeneous and inhomogeneous soil, as well as to different response modes.

By applying Eq. (27) to the soil profiles in Fig. 2 and using non-linear regression analysis of the Levenberg-Marquardt type over the range $10^2 < E_p/E_{sd} < 10^4$, the following relationship for the dimensionless parameters of the active pile length was obtained

$$\chi_L = \chi_1 - \chi_2 \log \varepsilon_{tol} \tag{28}$$

parameters χ_1, χ_2 and n_L are given in Table 2. The analysis reveals that the differences in the value of parameter χ_L in the literature could be attributed to the different tolerance limits adopted in different studies (Fig. 7).

It is worth mentioning that using the stiffness terms K_{rr} or K_{hr} instead of K_{hh} in Eq. (27), one obtains approximately the same results for L_a/d (not shown), which suggests that the effect of the response mode on active pile length is of minor importance.

Results for active pile length in various soil profiles obtained by means of Eq. (26) and Table 2 are illustrated in Fig. 7, plotted as a function of pile-soil stiffness contrast and different values of the tolerance parameter ε_{tol}. In the same plot, available solutions from the literature are shown for comparison. Evidently, L_a/d tends to increase with increasing E_p/E_{sd} and decrease with increasing ε_{tol}. The sensitivity of L_a in ε_{tol} leads to a difference of three to four diameters for $E_p/E_{sd} = 10^3$. The proposed solution is in meaningful agreement with those in the literature. An alternative interpretation of active pile length based on the value of dimensionless product (μL) is provided in Di Laora and Rovithis (2015).

STIFFNESS AND DAMPING COEFFICIENTS

Multi-layer profile

For a soil profile consisting of N homogeneous layers up to the active length, the integrals in Eqs. (16a,b) can be evaluated analytically. Expressed in terms of the dimensionless parameters S_{ij} (Eqs. 17, 18), the stiffness coefficients at the pile head are obtained as follows:

$$S_{hh} = \sum_{i=1}^{N} \left(\lambda_i/\mu\right)^4 \left\{-e^{-2\mu z}\left[2+\cos\left(2\mu z\right)+\sin\left(2\mu z\right)\right]\right\}_{z_{t,i}}^{z_{b,i}} \tag{29a}$$

$$S_{rr} = \sum_{i=1}^{N} \left(\lambda_i/\mu\right)^4 \left\{e^{-2\mu z}\frac{1}{3}\left[-2+\cos\left(2\mu z\right)-\sin\left(2\mu z\right)\right]\right\}_{z_{t,i}}^{z_{b,i}} \tag{29b}$$

$$S_{hr} = \sum_{i=1}^{N} \left(\lambda_i/\mu\right)^4 \left\{-e^{-2\mu z}\left[1+\sin\left(2\mu z\right)\right]\right\}_{z_{t,i}}^{z_{b,i}} \tag{29c}$$

The dimensionless coefficients associated with the radiation damping ($\beta^r_{ij} = \omega\ C^r_{ij} / (2K_{ij})$) are given below

$$w^r_{hh} = \frac{1}{1+S_{hh}} \sum_{i=1}^{N} \frac{\beta_{ri}}{\beta_{rd}} \left(\lambda_i/\mu\right)^4 \left\{-e^{-2\mu z}\left[2+\cos\left(2\mu z\right)+\sin\left(2\mu z\right)\right]\right\}_{z_{t,i}}^{z_{b,i}} \tag{30a}$$

$$w^r_{rr} = \frac{1}{1+S_{rr}} \sum_{i=1}^{N} \frac{\beta_{ri}}{\beta_{rd}} \left(\lambda_i/\mu\right)^4 \left\{e^{-2\mu z}\frac{1}{3}\left[-2+\cos\left(2\mu z\right)-\sin\left(2\mu z\right)\right]\right\}_{z_{t,i}}^{z_{b,i}} \tag{30b}$$

$$w^r_{hr} = \frac{1}{1+S_{hr}} \sum_{i=1}^{N} \frac{\beta_{ri}}{\beta_{rd}} \left(\lambda_i/\mu\right)^4 \left\{-e^{-2\mu z}\left[1+\sin\left(2\mu z\right)\right]\right\}_{z_{t,i}}^{z_{b,i}} \tag{30c}$$

with

$$\mu = \frac{1}{L_a} \sum_{i=1}^{N} \int_{h_{i-1}}^{L_a} \lambda_i\left(z\right) dz \tag{31}$$

in which $z_{t,i}$ denotes the elevation of the upper end of layer i, and $z_{b,i}$ denotes the elevation of the lower end (Fig. 2c); h_i is the thickness of the layer, λ_i is the corresponding pile wavenumber and β_{ri} (= $\omega\ c_{ri} / (2k_i)$) is the corresponding radiation damping coefficient. Eqs

(29) and (30) have been presented, in a different form, by Karatzia & Mylonakis (2012). The complementary coefficients $w_{ij}{}^{p}$ can be obtained from Eq. (22). The special case of a bilayer soil profile has been considered by Mylonakis (1995) and Mylonakis & Gazetas (1999).

Generalized parabolic profile

In case of a soil layer with parabolically varying modulus (a = arbitrary, n = arbitrary–Eq. 1), the corresponding coefficients are

$$S_{hh}=\frac{4\lambda_d^4}{\mu^4}2^{-\frac{3+n}{2}}\theta^{-n}e^{\theta a}\left\{2^{\frac{n+1}{2}}\Gamma_{10}-Q_{11}\cos\left[\frac{\pi(1+n)}{4}-\theta a\right]+B_{11}\sin\left[\frac{\pi(1+n)}{4}-\theta a\right]\right\} \tag{32a}$$

$$S_{rr}=\frac{8\lambda_d^4}{3\mu^4}2^{-\frac{5+n}{2}}\theta^{-n}e^{\theta a}\left\{2^{\frac{n+1}{2}}\Gamma_{10}-B_{11}\cos\left[\frac{\pi(1+n)}{4}-\theta a\right]-Q_{11}\sin\left[\frac{\pi(1+n)}{4}-\theta a\right]\right\} \tag{32b}$$

$$S_{hr}=\frac{4\lambda_d^4}{\mu^4}2^{-\frac{4+n}{2}}\theta^{-n}e^{\theta a}\left\{2^{\frac{n}{2}}\Gamma_{10}-Q_{11}\cos\left(\frac{\pi n}{4}-\theta a\right)+B_{11}\sin\left(\frac{\pi n}{4}-\theta a\right)\right\} \tag{32c}$$

$$w_{hh}^{r}=\frac{4\lambda_d^4}{\mu^4\left(1+S_{hh}\right)}2^{-\frac{6+n_1}{4}}\theta^{-\frac{n_1}{2}}e^{\theta a}\left\{2^{\frac{n_1+2}{4}}\Gamma_{20}-Q_{21}\cos\left[\frac{\pi(2+n_1)}{8}-\theta a\right]+B_{21}\sin\left[\frac{\pi(2+n_1)}{8}-\theta a\right]\right\} \tag{33a}$$

$$w_{rr}^{r}=\frac{8\lambda_d^4}{3\mu^4\left(1+S_{rr}\right)}2^{-\frac{10+n_1}{4}}\theta^{-\frac{n_1}{2}}e^{\theta a}\left\{2^{\frac{n_1+2}{4}}\Gamma_{20}-B_{21}\cos\left[\frac{\pi(2+n_1)}{8}-\theta a\right]-Q_{21}\sin\left[\frac{\pi(2+n_1)}{8}-\theta a\right]\right\}$$

$$w_{hr}^{r}=\frac{4\lambda_d^4}{\mu^4\left(1+S_{hr}\right)}2^{-\frac{8+n_1}{4}}\theta^{-\frac{n_1}{2}}e^{\theta a}\left\{2^{\frac{n_1}{4}}\Gamma_{20}-Q_{21}\cos\left[\frac{\pi n_1}{8}-\theta a\right]+B_{21}\sin\left[\frac{\pi n_1}{8}-\theta a\right]\right\} \tag{33b,c}$$

where $\theta = 2d\mu/(1-a)$ and Γ_{10}, Γ_{20}, Q_{11}, Q_{21}, B_{11}, B_{21} are dimensionless parameters provided in the Appendix. $n_1 = (1 - \xi)\, n$, ξ being 0 for frequency independent radiation damping as in Berger et al (1977) and Tabesh and Poulos (2000), and (–0.4) for the power law dependence of $a_0^{-0.4}$ in Eq. 10. λ_d is obtained from Eq. (13) and the corresponding shape parameter μ is given by

$$\mu=\frac{4\lambda_d}{(4+n)(a-1)}\left(\frac{L_a}{d}\right)^{-1}\left[a^{\frac{n+4}{4}}-\left(a+(1-a)\frac{L_a}{d}\right)^{\frac{n+4}{4}}\right] \tag{34}$$

The special cases of a soil profile whose Young's modulus increases linearly with depth (n = 1) and one having zero modulus at the soil surface (a = 0, $n \neq 0$) lead to simpler expressions which are provided in the Supplemental Data File.

Generalized exponential profile

For the variation in Young's modulus in Eq. (6) (Fig. 2b), the following closed-form expressions for the pile stiffness and damping were obtained

$$S_{hh} = \frac{k_\infty}{E_p I_p}\left\{\frac{3}{4\mu^4} + \frac{d(b-1)\left[(q+3d\mu)^2 + 3d^2\mu^2\right]}{\mu^3(q+2d\mu)\left[(q+2d\mu)^2 + (2d\mu)^2\right]}\right\} \tag{35a}$$

$$S_{rr} = \frac{k_\infty}{3E_p I_p}\left\{\frac{2b(2d\mu)^3 + q\left[(q+3d\mu)^2 + 7d^2\mu^2\right]}{4\mu^4(q+2d\mu)\left[(q+2d\mu)^2 + (2d\mu)^2\right]}\right\} \tag{35b}$$

$$S_{hr} = \frac{k_\infty}{E_p I_p}\left\{\frac{b(2d\mu)^2(q+4d\mu) + q\left[(q+3d\mu)^2 + 3d^2\mu^2\right]}{4\mu^4(q+2d\mu)\left[(q+2d\mu)^2 + (2d\mu)^2\right]}\right\} \tag{35c}$$

$$w_{hh}^r = \frac{\lambda_d^4\left[2A_0 + J_1 + J_2\right]}{\mu^4(1+S_{hh})\left[b+(1-b)(1-e^{-q})\right]^{n_2}} \tag{36a}$$

$$w_{rr}^r = \frac{\lambda_d^4\left[2A_0 + J_1 - J_2\right]}{3\mu^4(1+S_{rr})\left[b+(1-b)(1-e^{-q})\right]^{n_2}} \tag{36b}$$

$$w_{hr}^r = \frac{\lambda_d^4\left[2A_0 + J_1 - J_3\right]}{2\mu^4(1+S_{hr})\left[b+(1-b)(1-e^{-q})\right]^{n_2}} \tag{36c}$$

where dimensionless parameters A_0, J_1, J_2 and J_3 are defined in the Appendix. $n_2 = (1-\xi)/2$, ξ having the same meaning as before.

Shape parameter μ is given by

$$\mu = \frac{4d\lambda_d}{3qL_a\left[b+(1-b)(1-e^{-q})\right]^{1/4}}\left\{3b^{1/4} - \left(\frac{1}{b-1}\right)^{3/4} H_{p1} + \left[1+(b-1)e^{-\frac{qL_a}{d}}\right]^{1/4}\left(\frac{e^{\frac{qL_a}{d}}}{(b-1)}H_{p2} - 3\right)\right\} \tag{37}$$

where H_{p1} and H_{p2} are special functions provided in the Appendix.

The variations of S_{ij} and w^r_{ij} with the inhomogeneity parameters a and b obtained from Eqs (32), (33), (35) and (36) are depicted in Figs. 8 and 9. In the limit case where $a = b = 1$, the stiffness curves approach the values $S_{hh} = 3$, $S_{rr} = ⅓$ and $S_{hr} = 1$ corresponding to homogeneous soil conditions. Likewise, the radiation damping curves approach the values $w^r_{hh} = ¾$, $w^r_{rr} = ¼$ and $w^r_{hr} = ½$.

With reference to a generalized parabolic profile, Eqs (32) and (33) are presented graphically in Fig. 8 for three different inhomogeneity exponents (n= ¼, ½, 1) and pile-soil stiffness contrasts ($E_p/E_{sd} = 10^3, 10^4, 10^5$). The following noteworthy trends are evident: *First*, the stiffness coefficients S_{ij} invariably decrease with decreasing inhomogeneity parameter a and increasing n, being minimum for $n = 1$ (linear variation of Young's modulus with depth) and maximum for $n = 0$ (homogeneous soil conditions). *Second*, the ratio E_p/E_{sd} has minor effect on their values. *Third*, the rocking stiffness coefficient exhibits the smallest variation with the inhomogeneity parameters a and n over the other two coefficients. Similar observations can be made for the radiation damping coefficients w^r_{ij}, an exception being that the influence of ratio E_p/E_{sd} seems to be more important than in the stiffness terms.

The impedance coefficients of a pile embedded in a soil profile with exponentially varying stiffness are illustrated in Fig. 9. In this case, Eqs (35) and (36) are plotted considering three different inhomogeneity parameters (q = ¼, ½, 1) and three pile-soil stiffness ratios ($E_p/E_{sd} = 10^3, 10^4, 10^5$). It is observed that the stiffness coefficients S_{ij} tend to decrease with decreasing values of b and q, the trend being more pronounced in the swaying mode. With respect to pile-soil stiffness contrast, stiffness coefficients increase with E_p/E_{sd}. On the other hand, coefficients w^r_{ij} invariably increase with decreasing b, q and E_p/E_{sd}. The results of Figs. 8 and 9 can be used in practical applications, as they cover a wide set of cases without having to numerically evaluate Eqs (32), (33), (35) and (36).

The variation with pile-soil stiffness contrast of coefficients K_{hh}, K_{rr} and K_{hr} obtained from the proposed formulation is plotted in Fig. 10 for a linear and a parabolic soil profile, n=1, a=0 and n=½, b=0, respectively. In the same plot, results from available solutions from the literature are shown for comparison. The stiffness coefficients are normalized with respect to $E_{sd}\, d^{\,l}$, the value of the exponent l being 1, 2 or 3 depending on the oscillation mode. The accord between the proposed analytical solution and the empirical formulas is satisfactory.

A comparison of the damping coefficients obtained from the proposed closed-form solution with those from the empirical solutions of Gazetas (1991) and Syngros (2004) is provided in Fig. 11 for linear soil stiffness variation with depth. Damping coefficients are plotted against dimensionless frequency a_{0d} (= $\omega d/V_{sd}$) corresponding to a depth of one pile diameter. The analytical solution compares favorably with the empirical solutions. Also plotted in Fig. 11 are results obtained by means of Eq. (20), based on different formulas for the radiation damping coefficient c_r.

APPLICATION EXAMPLE

Gazetas and Dobry (1984) presented an illustrative example of a floating pile embedded in a realistic multi-layer soil profile. An almost identical soil stratification is depicted in Fig.12, and is typical of those existing in the San Francisco Bay Area. The soil deposit resting on bedrock has ~60 m depth and consists of seven main layers, whose composition varies from sandy fill at the surface, to stiff and very stiff clays at depth. A 1.4m diameter concrete-filled steel-pipe pile of 0.085 m pipe thickness, embedded in the upper 34 m of the soil stratum is studied. The pile is subjected to lateral dynamic loading with frequency f ranging from 0 to 22 Hz.

The Young's modulus of an equivalent solid homogeneous pile having the same flexural stiffness E_pI_p as the actual pile is

$$\tilde{E}_p = E_{st}\left[1-\left(1-\frac{2t_w}{d}\right)^4\left(1-\frac{E_c}{E_{st}}\right)\right] = 2.5\cdot 10^8\left[1-\left(1-\frac{2\cdot 0.085}{1.4}\right)^4\left(1-\frac{2.5\cdot 10^7}{2.5\cdot 10^8}\right)\right] = 1.15\cdot 10^8 \ kPa \quad (38)$$

Step 1: The active pile length should be determined considering the soil inhomogeneity. As a first approximation, the solution corresponding to linear inhomogeneity with depth (n = 1) will be utilized. Thus, L_a is computed by means of Eq. (26) selecting the parameters for a linear profile (Table 2), with tolerance $\varepsilon_{tol} = 10^{-2}$, $E_p/E_{sd} = 1.15\times10^8/1.32\times10^5 = 870$, to get the estimate L_a = 10.4m (~7d). This suggests that the first two layers, the thick sandy fill and the normally consolidated San Francisco Bay Mud, mainly contribute to the lateral response of pile. Therefore, the stiffness and damping coefficients are obtained using Eqs (29)-(30) considering the contribution of the upper two soil layers, with each layer having constant Young's modulus, i.e., E_{s1} = 132 MPa and E_{s2} = 86 MPa, respectively. Accordingly, the pile-soil stiffness ratio E_p/E_{sd} required for computing L_a is 870. Remarkably, the resulting active length is half of that predicted in the original example based on dynamic considerations.

Step 2: The Winkler constant for each layer is obtained by means of Eqs (23) and (25) selecting the parameters for homogeneous profile (Table 1), to get δ =1.35 as an average value in the first two layers.

Step 3: The Winkler parameters corresponding to the surface upper and the underlying layer are obtained by applying Eq (13), to be found λ_1 = 0.213 m^{-1} and λ_2 = 0.191 m^{-1}, respectively. Accordingly, the shape parameter (Eq 31) attains the anticipated average value

$$\mu = \frac{1}{10.4}\left[4.2\cdot 0.213 + (10.4-4.2)0.191\right] = 0.2\ m^{-1} \quad (39)$$

Step 4: The stiffness coefficients S_{ij} are computed by evaluating Eqs (29a-c) as follows

$$S_{hh} = \left(\frac{0.213}{0.2}\right)^4\left\{-e^{-2\cdot 0.2\cdot z}\left[2+\cos(2\cdot 0.2\cdot z)+\sin(2\cdot 0.2\cdot z)\right]\right\}_0^{4.2} + \\ +\left(\frac{0.191}{0.2}\right)^4\left\{-e^{-2\cdot 0.2\cdot z}\left[2+\cos(2\cdot 0.2\cdot z)+\sin(2\cdot 0.2\cdot z)\right]\right\}_{4.2}^{10.4} = 3.61 \quad (40a)$$

$$S_{rr}=\left(\frac{0.213}{0.2}\right)^4\left\{e^{-2\cdot0.2\cdot z}\,\frac{1}{3}\left[-2+\cos\left(2\cdot0.2\cdot z\right)-\sin\left(2\cdot0.2\cdot z\right)\right]\right\}_0^{4.2}+$$
$$+\left(\frac{0.191}{0.2}\right)^4\left\{e^{-2\cdot0.2\cdot z}\,\frac{1}{3}\left[-2+\cos\left(2\cdot0.2\cdot z\right)-\sin\left(2\cdot0.2\cdot z\right)\right]\right\}_{4.2}^{10.4}=0.33 \qquad (40b)$$

$$S_{hr}=\left(\frac{0.213}{0.2}\right)^4\left\{-e^{-2\cdot0.2\cdot z}\left[1+\sin\left(2\cdot0.2\cdot z\right)\right]\right\}_0^{4.2}+$$
$$+\left(\frac{0.191}{0.2}\right)^4\left\{-e^{-2\cdot0.2\cdot z}\left[1+\sin\left(2\cdot0.2\cdot z\right)\right]\right\}_{4.2}^{10.4}=1.12 \qquad (40c)$$

where the subscripts and superscripts following the curly braces denote difference between values at two elevations.

Step 5: By substituting the predicted stiffness coefficients S_{ij} to Eqs (18a-c) yields the stiffness values K_{hh} = 0.8×10^6 kN/m, K_{rr} = 8.7×10^6 kNm and K_{hr} = 1.8×10^6 kN. K_{hh} deviates by a mere 10% from the finite-element result reported by Gazetas and Dobry (1984).

Step 6: It is straightforward to obtain the dimensionless weight factors w^p_{ij} via Eq. (22), i.e., w^p_{hh} = 0.22, w^p_{rr} = 0.75, w^p_{hr} = 0.47.

Step 7: As for the radiation damping coefficient β_r, Eqs. (10) and (21) are utilized, keeping in mind that the properties are constant within each layer. In the first layer, using V_s/V_c = 0.61 corresponding to ν = 0.25, Eq. (10) yields

$$c_{r1} = 1.4\cdot\pi\cdot1.85\cdot169\cdot(0.25 + 0.8\cdot0.61^{-1})\cdot(2\,\pi f\cdot1.4/169)^{-0.4}\cong 7000\,f^{-0.4} \quad \text{(kPa·s)} \qquad (41a)$$

For the second layer, using V_s/V_c = 0.5, Eq. (10) provides

$$c_{r2} = 1.4\cdot\pi\cdot1.7\cdot130\cdot(0.25 + 0.8\cdot0.5^{-1})\cdot(2\,\pi f\cdot1.4/130)^{-0.4}\cong 5300\,f^{-0.4} \quad \text{(kPa·s)} \qquad (41b)$$

Since k_1=1.35×1.32×10^5=1.8×10^5 kPa and k_2=1.35×0.86×10^5=1.2×10^5 kPa, Eq.(21) yields

$$\beta_{r1}=\frac{2\cdot\pi\cdot f}{2\cdot1.8\cdot10^5}\cdot7000\cdot f^{-0.4}=0.122\,f^{0.6},\quad \beta_{r2}=\frac{2\cdot\pi\cdot f}{2\cdot1.2\cdot10^5}\cdot5300\cdot f^{-0.4}=0.139\,f^{0.6} \qquad (42a,b)$$

Step 8: In the same vein and using $\beta_{rd} = \beta_{r1}$, damping coefficients w^r_{ij} (Eq. 30) are estimated as w^r_{hh} = 0.79, w^r_{hr} = 0.55, w^r_{rr} = 0.27.

Step 9: Applying Eq. (20) leads to the following expressions

$$\beta_{hh} = 0.22 \cdot 0.02 + (1-0.22) \cdot 0.04 + 0.79 \cdot 0.122 f^{0.6} = 0.036 + 0.096 f^{0.6} \quad (43a)$$

$$\beta_{hr} = 0.47 \cdot 0.02 + (1-0.47) \cdot 0.04 + 0.55 \cdot 0.122 f^{0.6} = 0.031 + 0.067 f^{0.6} \quad (43b)$$

$$\beta_{rr} = 0.75 \cdot 0.02 + (1-0.75) \cdot 0.04 + 0.27 \cdot 0.122 f^{0.6} = 0.025 + 0.033 f^{0.6} \quad (43c)$$

For simplicity, a fixed value $\beta_s = 0.04$ is adopted for the soil material damping pertaining to the sand material in the upper soil layer. The damping coefficients are illustrated in Fig.13.

Alternative Solution for Linear Profile

The same problem may be solved by replacing the actual multi-layer soil profile with an equivalent idealized linear profile. Although this is not essential in the present case (where adequate information for the subsoil is available) the example is solved on the basis of this assumption to demonstrate the applicability of the proposed method and facilitate understanding of the various steps.

Without loss of accuracy, the variation of Young's modulus within the actual soil deposit can be described by the linear function of depth obtained using linear regression, (Fig.12),

$$E_s(z) = 85.6\ (0.85 + 0.11z)\ \text{MPa} \quad (44)$$

Note that performing the regression within a shallower range, say within the upper one third of the pile, corresponding to the active length, does not significantly alter the results. To determine the impedance at the pile head, one may utilize the expressions for stiffness and damping coefficients pertaining to the generalized parabolic profile ($a \neq 0$, $n \neq 0$).

Step 1: According to the proposed method, the inhomogeneity parameters a and n, and the reference Young's modulus at depth of one pile diameter are first evaluated at $E_{sd} = 85.6$ MPa, $a = E_{s0}/E_{sd} \cong 0.85$, $n = 1$, resulting from matching Eqs (1) and (44).

Step 2: Having determined the ratio $E_p/E_{sd} = 1.15\times10^8/0.856\times10^5 = 1.34\times10^3$, L_a is given by Eq. (26) and Table 2, considering the same parameters as before (assuming tolerance $\varepsilon_{tol} = 10^{-2}$), to get $L_a = 11$m (~8d).

Step 3: From Eqs (23) and (25) and choosing the values $\chi_\delta = 1.633$ and $n_\delta = -0.2$ from Table 1, pertaining to linear soil stiffness variation with depth, fixed head piles and $v = 0.4$, parameter δ is estimated at 1.74.

Step 4: Using $a = 0.85$, $n = 1$ and $\lambda_d = 0.2$ m^{-1}, the shape parameter μ obtained from Eq (34) is obtained at 0.22 m^{-1}.

Step 5: Stiffness coefficients are given by Eqs (32a-c). Parameter θ is found to be 4.15, while via Eq. 52b and setting $n^* = n = 1$, parameters Γ_{10}, Γ_{11}, B_{11} and Q_{11} are estimated to be

$$\Gamma_{10} = (4.15\cdot 0.85)e^{-4.15\cdot 0.85}[1+1/(4.15\cdot 0.85)] = 0.13 \tag{45a}$$

$$\Gamma_{11} = [4.15\cdot 0.85\cdot(1+i)]e^{-4.15\cdot 0.85\cdot(1+i)}\{1+1/[4.15\cdot 0.85\cdot(1+i)]\} = -0.162 - 0.045i \tag{45b}$$

$$B_{11} = \mathrm{Re}[\Gamma_{11}] = -0.162,\ Q_{11} = \mathrm{Im}[\Gamma_{11}] = -0.045 \tag{45c,d}$$

The application of Eqs (32a-c) using the above values yields

$$S_{hh} = \frac{4\cdot 0.2^4}{0.22^4}\cdot 2^{-2}\cdot 4.15^{-1}\cdot e^{4.15\cdot 0.85}\times \\ \times\left[2\cdot 0.13+0.045\cdot\cos\left(\pi/2-4.15\cdot 0.85\right)-0.162\cdot\sin\left(\pi/2-4.15\cdot 0.85\right)\right]=2.3 \tag{46a}$$

$$S_{rr} = \frac{8\cdot 0.2^4}{3\cdot 0.22^4}\cdot 2^{-3}\cdot 4.15^{-1}\cdot e^{4.15\cdot 0.85}\times \\ \times\left[2\cdot 0.13+0.162\cdot\cos\left(\pi/2-4.15\cdot 0.85\right)+0.045\cdot\sin\left(\pi/2-4.15\cdot 0.85\right)\right]=0.31 \tag{46b}$$

$$S_{hr} = \frac{4\cdot 0.2^4}{0.22^4}\cdot 2^{-\frac{5}{2}}\cdot 4.15^{-1}\cdot e^{4.15\cdot 0.85}\times \\ \times\left[2^{1/2}\cdot 0.13+0.045\cdot\cos\left(\pi/4-4.15\cdot 0.85\right)-0.162\cdot\sin\left(\pi/4-4.15\cdot 0.85\right)\right]=0.85 \tag{46c}$$

which suggest that soil contributes 2.3, 0.31 and 0.85 times the amount of stiffness provided by the pile element in swaying, rocking and cross swaying-rocking, respectively.

Step 6: Eqs (18a-c) provide the stiffness values $K_{hh} = 0.79\times 10^6$ kN/m, $K_{rr} = 9.5\times 10^6$ kNm and $K_{hr} = 2\times 10^6$ kN. These results are in good agreement with those obtained using the multi-layer actual profile with discrepancies of 1%, 8% and 10%, respectively.

Using the simpler expressions provided in the Supplemental Data File (Eq. S9) yields

$$S_{hh} = \frac{3 \cdot 0.2^4}{2 \cdot 1.4 \cdot 0.22^5}\left[1 + 0.85\left(2 \cdot 1.4 \cdot 0.22 - 1\right)\right] = 2.24 \quad (47a)$$

$$S_{rr} = \frac{0.2^4}{3 \cdot 1.4 \cdot 0.22^5}\left[1 + 0.85\left(1.4 \cdot 0.22 - 1\right)\right] = 0.3 \quad (47b)$$

$$S_{hr} = \frac{0.2^4}{4 \cdot 1.4 \cdot 0.22^5}\left[3 + 0.85\left(4 \cdot 1.4 \cdot 0.22 - 3\right)\right] = 0.83 \quad (47c)$$

which practically coincide with results in Eq. (46) (differences being due to cut-off errors).

Step 7: Applying an analogous procedure for the coefficients w^r_{ij}, using $n_1 = (1 - (-0.4)) \times 1 = 1.4$, Eqs (33a-c) lead to $w^r_{hh} = 0.67$, $w^r_{rr} = 0.21$, $w^r_{hr} = 0.42$. Eq. (22) provides the coefficients w^p_{ij}, associated with the pile material damping, i.e, $w^p_{hh} = 0.30$, $w^p_{rr} = 0.76$, $w^p_{hr} = 0.54$.

Step 8: Subsequently, the dashpot coefficient c_r (Eq. 10) computed at depth of one pile diameter according to Eq. (21) is estimated to be

$$c_{rd} = 1.4 \cdot \pi \cdot 1.85 \cdot 129 \cdot (0.25 + 0.8 \cdot 0.5^{-1})(2\pi f\, 1.4/129)^{-0.4} \cong 5200\, f^{-0.4} \quad \text{(kPa·s)} \quad (48)$$

Step 9: Considering $k_d = 1.5 \times 10^5$ kPa, the radiation damping coefficient is $\beta_{rd} = 0.11 f^{0.6}$.

Step 10: Finally, the expressions for the dimensionless damping coefficients are

$$\beta_{hh} = 0.034 + 0.074\, f^{0.6},\ \beta_{hr} = 0.029 + 0.048\, f^{0.6},\ \beta_{rr} = 0.025 + 0.024\, f^{0.6} \quad (49a\text{-}c)$$

Alternative Solution for an Exponential Profile

As a second alternative, an idealized exponential soil profile is employed.

Step 1: It is assumed that $E_{s\infty} = 480$ MPa, thus $b = E_{s0}/E_{s\infty} = 58/480 \cong 0.1$, and $q = 0.1$. The stiffness variation with depth z, depicted in Fig.12, is

$$E_s(z) = 480\ [0.1 + 0.9\ (1 - e^{-0.07z})] \text{ MPa} \quad (50)$$

Step 2: Considering $E_p/E_{sd} = 1.15 \times 10^8 / 0.89 \times 10^5 = 1.3 \times 10^3$, L_a is obtained by Eq. (26) and Table 2, assuming $\varepsilon_{tol} = 10^{-2}$, at $L_a = 12$m (~8.5d).

591 *Step 3*: From Eqs. (23) and (25) and using the values $\chi_\delta = 1.34$ and $n_\delta = -0.23$ from Table 1,
592 for an exponential soil profile and a fixed head pile, parameter δ is estimated at 1.4 (Poisson's
593 ratio taken equal to 0.4).
594 *Step 4*: Using $b = q = 0.1$, and $\lambda_d = 0.19$ m^{-1}, the shape parameter μ (Eq. 37) is 0.23 m^{-1}.
595 *Step 5*: From Eqs. (35a-c) with $k_\infty = 1.4\times4.8\times10^5 = 6.7\times10^5$ kPa, it is straightforward to obtain
596 the stiffness coefficients $S_{hh} = 1.84$, $S_{rr} = 0.30$ and $S_{hr} = 0.77$.
597 *Step 6*: Evaluating Eqs. (18a-c) yield the stiffnesses $K_{hh} = 0.75\times10^6$ kN/m, $K_{rr} = 9.7\times10^6$ kNm
598 and $K_{hr} = 2\times10^6$ kN, which are very similar to those obtained above and highlight the
599 insensitivity of the solution to soil stiffness at depth.
600 *Step 7*: Using again $n_2 = (1-(-0.4)) / 2 = 0.7$, parameters A_0, J_1, J_2 and J_3 are numerically
601 evaluated using standard mathematical software at $A_0 = 0.34$, $J_1 = 0.066$, $J_2 = 0.288$ and $J_3 =$
602 -0.066. Substituting the above values into Eqs. (36a-c) yields $w^r_{hh} = 0.55$, $w^r_{rr} = 0.18$, $w^r_{hr} =$
603 0.35, while Eq. (22) yields $w^p_{hh} = 0.35$, $w^p_{rr} = 0.77$, $w^p_{hr} = 0.56$.
604 *Step 8*: Evaluating Eq. (10) leads to $c_{rd} \cong 5300\, f^{-0.4}$ kPa·s (similar result with linear profile).
605 *Step 9*: Considering $k_d = 1.2\times10^5$ kPa, the radiation damping coefficient is $\beta_{rd} = 0.14 f^{0.6}$.
606 *Step 10*: Finally, the expressions for the dimensionless damping coefficients are
607 $$\beta_{hh} = 0.033+0.078\, f^{0.6},\ \beta_{hr} = 0.029+0.049\, f^{0.6},\ \beta_{rr} = 0.025+0.025\, f^{0.6} \qquad (51a\text{-}c)$$
608

609 ## CONCLUSIONS

610 An approximate, practically-oriented analysis procedure was developed for estimating the
611 dynamic stiffness and damping (impedance coefficients) of a laterally-loaded pile in different
612 types of vertically inhomogeneous soil. To this end, a dynamic Winkler model was adopted
613 in conjunction with a virtual-work scheme associated with approximate shape functions for
614 the pile deflection under imposed head displacements and rotations. Two auxiliary models for

615 determining the moduli of the distributed Winkler springs and dashpots were also outlined.
616 The main conclusions of the study are:

617 1. The proposed analytical technique allows closed-form solutions for the pile stiffness and
618 damping at the pile head to be obtained for both bounded and unbounded, layered soil and
619 soil whose stiffness varies smoothly with depth. Results are provided in dimensionless
620 form, which sheds light into the physics of the problem, including the relative
621 contributions to overall stiffness and damping of the pile and soil components. The insight
622 offered by this modular approach is hardly possible with rigorous numerical solutions such
623 as finite elements.
624 2. Unlike earlier approximate methods, where a limited number of impedance coefficients
625 are determined, this work covers all six impedance coefficients (i.e., K_{hh}, K_{rr}, K_{hr}, C_{hh}, C_{rr},
626 C_{hr}) in different soil profiles. The method is self-standing and does not involve empirical
627 information. The solutions have been further improved by employing enhanced
628 expressions for various parameters as summarized in the following.
629 3. A new model was developed for the distributed Winkler radiation damping coefficient
630 based on a 2D plane strain infinitesimal sector idealization. It was found that, contrary to
631 trends suggested by existing formulae, the dashpot coefficient does not tend to zero at high
632 frequencies, but approaches asymptotically the value $c_r = 1.4\, d\, \pi\, \rho_s\, V_s$. On the other hand,
633 the 2D plane strain stiffness k goes to zero both at low and high frequencies.
634 4. A new analytical formulation was developed for the distributed Winkler spring coefficient
635 along the pile, extending an earlier 3D elasticity model by the senior author. In
636 homogeneous soil, Winkler modulus k varies between 1–2 E_s for both fixed- and free-head
637 piles, whereas for inhomogeneous soil, $k \approx$ 1–2 E_{sd} for fixed-head and 1.5–3 E_{sd} for free-
638 head piles.

5. A novel solution (Eqs. 26-27, Table 2) was derived for the active pile length in different soil profiles. The associated correlation coefficients encompass a tolerance parameter (ε_{tol}) which helps to explain discrepancies in the results reported in the literature. For E_p/E_{sd} values in the range 10^2 and 10^3, L_a varies between 5 and 13d. The largest L_a occurs in homogeneous soil, and the smallest in a linear profile.
6. Results for pile stiffness and damping obtained with the proposed method are in good agreement with available numerical solutions and fitted formulae. Coefficients S_{ij} indicate that in the lateral mode soil contributes to the overall stiffness between 1 and 3 times the stiffness provided by the pile. In the other two modes the soil contribution is much smaller, ranging between 0.4 and 1 in cross swaying-rocking and 0.17 to 0.34 in rocking.
7. The proposed method can be implemented by means of hand calculations or simple computer spreadsheets and, thereby, can be used in routine calculations for designing piles against lateral dynamic loads.

As a final remark, it is noted that nonlinear effects such as those described by *p-y* curves can be readily incorporated in the solution, via iterative application of the equations of the layered profile until convergence is achieved. Such applications lie beyond the scope of this work.

APPENDIX: PARAMETERS FOR STIFFNESS & DAMPING COEFFICIENTS

In Eqs (32) and (33) parameters Γ_{10}, Γ_{20}, $B_{11} = Re[\Gamma_{11}]$, $B_{21} = Re[\Gamma_{21}]$, $Q_{11} = Im[\Gamma_{11}]$, $Q_{21}=Im[\Gamma_{21}]$ are obtained from the generalized Gamma function

$$\Gamma_{op} = \Gamma\left[\frac{n^* + o}{o}, \frac{2da\mu}{1-a}(1+ip)\right] \quad , \quad o = 1,2 \, , \, p = 0,1 \tag{52a}$$

with n^* being n and n_1 for stiffness and damping coefficients, respectively. For $a = 0$, it can be approximated by Stirling's formula (see Supplemental Data File); for $a > 0.5$ the following approximation applies (Abramowitz & Stegun 1965)

$$\Gamma_{op} \approx \left[\theta a\left(1+i\,p\right)\right]^{\frac{n^*}{o}} e^{-\theta a(1+i\,p)}\left\{1+\frac{n^*}{o\theta a\left(1+i\,p\right)}\right\},\quad o=1,2\,,\ p=0,1 \tag{52b}$$

In Eqs (36a-c) parameters A_0, $J_1=Im[A_{-1}]$, $J_2=Re[A_{-1}]$ and $J_3=Im[A_1]$ are denoted as

$$A_{t^*} = {}_2F_1\left[-n_2,\left(1+i\,t^*\right)2d\mu/q;1+\left(1+i\,t^*\right)2d\mu/q;1-b\right] \tag{53}$$

with A_{t^*} being a hypergeometric function in which the subscript t^* takes the values −1, 0 and 1.

In Eq. (37) parameters H_{p1} and H_{p2} denote the following hypergeometric functions

$$H_{p1} = {}_2F_1\left(\frac{3}{4},\frac{3}{4},\frac{7}{4};\frac{1}{1-b}\right) \qquad , \qquad H_{p2} = {}_2F_1\left[1,1,\frac{7}{4};e^{\frac{qL_a}{d}}/\left(1-b\right)\right] \tag{54a,b}$$

which can be evaluated using standard computer software such as Matlab and Mathematica.

NOTATION

The following symbols are used in this paper:

Latin symbols

A_{t^*} = hypergeometric function

a_0 = dimensionless frequency

a_{0d} = dimensionless frequency at depth $z = d$

B_{11}, B_{21} = real part of generalized Gamma functions Γ_{11} and Γ_{21}, respectively

b = dimensionless inhomogeneity parameter for exponential soil profile

C_{hh}, C_{rr}, C_{hr}, C_{ij} = damping coefficients in swaying, rocking and cross swaying-rocking at pile head

c_r, $c_r(z)$ = Winkler radiation dashpot modulus

c_{rd} = Winkler radiation dashpot modulus at depth of one pile diameter

c_{ri} = dashpot modulus of soil layer i

d = pile diameter

E_s, $E_s(z)$ = soil Young's modulus

E_{s0}, E_{sd}, $E_{s\infty}$ = soil Young's modulus at soil surface, at depth of one pile diameter, and at infinite depth, respectively

E_p = pile Young's modulus

E_pI_p = pile flexural stiffness

E_c, E_{st} = Young's modulus of concrete and steel pile, respectively

$\tilde{E}_p$ = Young's modulus of an equivalent solid non hollow pile

692 f = excitation frequency

693 G_s, $G_s(z)$ = soil shear modulus

694 $H_0^{(2)}$, $H_1^{(2)}$ = zero- and first-order Hankel functions of the second kind

695 H_{p1}, H_{p2} = hypergeometric functions

696 h_i = thickness of soil layer i

697 i = imaginary unit, number of soil layer in multilayered soil (subscript)

698 ij = refers to different vibrational modes

699 J_1, J_2 = imaginary and real part of hypergeometric function A_{-1}, respectively

700 J_3 = imaginary part of hypergeometric function A_1

701 k, $k(z)$ = Winkler spring modulus

702 k_d, k_∞ = Winkler spring modulus at depth $z = d$ and at infinite depth, respectively

703 k_i = Winkler spring modulus of soil layer i

704 K_{hh}, K_{rr}, K_{hr}, K_{ij} = pile head stiffness coefficients in swaying, rocking and cross swaying-rocking at

705 pile head

706 K^p_{ij} = contribution to overall head stiffness of pile flexural stiffness

707 L = pile length

708 L_a = active pile length

709 l = exponent 1, 2 or 3 depending on oscillation mode

710 m = pile mass per unit length

711 N = number of homogeneous layers

712 n = dimensionless inhomogeneity exponent for generalized parabolic soil profile

713 n_1, n_2, n^* = dimensionless parameters

714 n_δ, n_L = dimensionless coefficients

715 o, p = arguments of generalized Gamma function

716 q = dimensionless inhomogeneity exponent for exponential soil profile

717 Q_{11}, Q_{21} = imaginary part of generalized Gamma functions Γ_{11} and Γ_{21}, respectively

718 S_{ij} = dimensionless stiffness coefficient expressing the contribution of the restraining

719 action of soil to the overall head stiffness

720 t = time

721 t_w = wall thickness of hollow pile

722 t^* = argument of hypergeometric function

723 V_c = soil compressional wave propagation velocity

724 V_s = soil shear wave propagation velocity

725 V_{sd} = soil shear wave velocity at depth of one pile diameter

726 V_{La} = Lysmer's analog wave propagation velocity

727 w^p_{ij},w^r_{ij} = weight factors expressing the contribution of pile material and radiation damping,

728 respectively, to the overall damping
729 Y_o = amplitude of motion at pile head
730 Y, $Y(z)$ = pile deflection
731 z = depth
732 $z_{t,i}$, $z_{b,i}$ = elevation of upper (t) and lower (b) face of soil layer i
733 **Greek symbols**
734 a = dimensionless inhomogeneity parameter for generalized parabolic soil profile
735 a_c = dimensionless stiffness parameter
736 β_p = pile hysteretic damping
737 β_s = soil hysteretic damping
738 β_{rd} = radiation damping coefficient at depth of one pile diameter
739 β_{ij} = normalized damping coefficients at pile head
740 β_{ri} = dimensionless damping coefficient of soil layer i
741 γ = Euler's number ($\cong 0.577$)
742 Γ_{op} = generalized Gamma function
743 δ = Winkler spring coefficient
744 ε_{tol} = tolerance parameter
745 ε_z = vertical normal strain
746 η_u = compressibility coefficient
747 θ = dimensionless coefficient
748 λ, $\lambda(z)$ = Winkler wavenumber parameter (1/Length)
749 λ_d = Winkler wavenumber parameter at depth of one pile diameter
750 λ_i, $\lambda_i(z)$ = Winkler wavenumber parameter of soil layer i
751 Λ = complex-valued dimensionless function of frequency
752 μ = shape parameter
753 ν = soil Poisson's ratio
754 ξ = dimensionless parameter
755 ρ_s = soil mass density
756 σ_z = vertical normal stress
757 ϕ = polar angle in global reference system
758 $\varphi(z)$ = normalized deflected shape of a fixed-head pile due to unit head rotation under zero
759 displacement
760 $\chi(z)$ = normalized deflected shape of a fixed-head pile due to unit head displacement under
761 zero rotation
762 χ_i, χ_j = any of the shape functions $\chi(z)$ and $\varphi(z)$
763 χ_δ, χ_L, χ_1, χ_2 = dimensionless coefficients

764 $\psi(z)$ = normalized deflected shape of a free-head pile due to a horizontal head force
765 ω = cyclic excitation frequency
766

767 ## ACKNOWLEDGEMENTS

768 The authors would like to acknowledge the contributions, in chronological order, of Mr.
769 Dimitri Roumbas, Dr. Costis Syngros, Ms. Alkisti Zina, Mr. Stefanos Drosos and Dr. Panos
770 Papastylianou, all former students of the senior author at the City University of New York
771 and University of Patras, in the development of the above method. Partial funding received
772 through a Caratheodory Program (B.388) at University of Patras is gratefully acknowledged.
773

774 ## REFERENCES

775 Abramowitz, M., and Stegun, I. A. (1965), *Handbook of Mathematical Functions*, U.S. National
776 Bureau of Standards (1964); Dover, New York
777 Anoyatis, G. and Mylonakis, G. (2012). "Dynamic Winkler Modulus for Axially Loaded Piles",
778 Geotechnique, 62 (6), 521-536.
779 Anoyatis, G., Mylonakis, G. and Lemnitzer, A. (2016). "Soil reaction to lateral harmonic pile
780 motion", J. Soil Dynamics and Earthquake Engineering, 87, 164-179.
781 Banerjee, P.K. and Davis, T.G. (1978). "The behaviour of axially and laterally loaded single piles
782 embedded in non – homogeneous soils", Geotechnique, 28(3), 309-326.
783 Basu, D. and Salgado, R. (2008). "Analysis of laterally-loaded piles with rectangular cross sections
784 embedded in layered soil media", Int. J. Num. Anal. Meth. Geomech., 32(7), 721-744.
785 Berger, E., Mahin, S. A., and Pyke, R. (1977), "Simplified Method for Evaluating Soil-Pile Structure
786 Interaction Effects," *Proc., 9th Offshore Technology Conf.,* OTC Paper 2954, Houston, Tex., 589-598.
787 Bevington, P. R. and Robinson, D. K. (1992). "Data reduction and error analysis for the physical
788 sciences." New York: McGraw Hill.
789 Blaney, G. W., Kausel, E., and Roesset, J. M. (1976), "Dynamic Stiffness of Piles," Proc. 2^{nd} *Int.*
790 *Conf. Num. Meth. Geomech.,* Vol. II, Blacksburg, Virginia, June, 1001-1012.

791 Budhu, M, and Davis, T. G. (1987). "Nonlinear analysis of laterally loaded piles in cohesionless
792 soils", Can. Geotech. J., 24, 289-296.
793 Clough R.. W. & Penzien, J. (1975). *Structural Dynamics*, McGraw-Hill.
794 Darendeli M. (2001). "Development of a new family of normalized modulus reduction and material
795 damping curves." Ph.D. Thesis, Dept. of Civil Eng. University of Texas, Austin.
796 Di Laora, R. and Rovithis, E. (2015). "Kinematic bending of fixed-head piles in nonhomogeneous
797 soil", J. Geotech. Geoenviron. Eng. 141(4) 04014126, DOI: 10.1061/(ASCE) GT.1943-5606.0001270
798 Dobry, R., Vicente, E., O'Rourke, M. J., and Roesset, J. M. (1982)."Horizontal stiffness and damping
799 of single piles", J. Geotech. Eng. Div., ASCE, Vol. 108, No. GT3, 439-459
800 El-Marsafawi, H., Kaynia, H.M., and Novak, M. (1992). "Interaction factors and the superposition
801 method for pile group dynamic analysis", Report GEOT-1-92, GRC, Univ. Western Ontario, Canada.
802 Fleming, W.G.K., Weltman, A.J., Randolph, M.F., Elson, W.K. (1993). *Piling Enineering*, 2nd
803 Edition, John Wiley & Sons.
804 Gazetas, G. (1991). "Foundation Vibrations", in Foundation Engineering Handbook, (H.Y. Fang, ed.),
805 Van Nostrand Reinholds, New York, 553-593.
806 Gazetas, G. and Dobry, R. (1984). "Horizontal response of piles in layered soils". J. Geotech. Eng.
807 Div., ASCE, 110, 20-40.
808 Gazetas, G. and Mylonakis, G. (1998). "Seismic Soil-Structure Interaction: New Evidence and
809 Emerging Issues", Geotechnical Special Publication No. 75, ASCE, 1119-1174.
810 Gerber M. T. and Rollins M. K. (2008). "Cyclic P-Y Curves for a Pile in Cohesive Soil." Proc. Of
811 Geotech. Earthquake Eng. and Soil Dyn., IV, 1-10.
812 Gerolymos N. and Gazetas G. (2005b). "Phenomenological model applied to inelastic response of
813 soil–pile interaction systems". Soils and Foundations, 45(4), 119–132.
814 Guo, W. (2012). *Theory and Practice of Pile Foundations*. London: CRC Press.
815 Hetenyi, M. (1946). *Beams on elastic foundation*, University of Michigan Press.
816 Kaynia, A. M., and Kausel, E. (1982). "Dynamic behaviour of pile groups", Proc. of the 2nd Int. Conf.
817 on Numerical Methods in Offshore Piling, University of Texas at Austin, 509-531.

818 Karatzia X. and Mylonakis G. (2012). “Horizontal response of piles in inhomogeneous soil: simple
819 analysis”. Proc. 2nd Int. Con. on PBD in Earth. Geotech. Eng., No 1117, Taormina, Italy.
820 Karatzia X., Papastylianou P. and Mylonakis G. (2014). “Horizontal Soil Reaction of a Cylindrical
821 Pile Segment with a Soft Zone”. J. Eng. Mech., 10.1061/(ASCE)EM.1943-7889.0000792.
822 Karatzia, X., Papastylianou, P., and Mylonakis, G. (2015). "Erratum for “Horizontal Soil Reaction of
823 a Cylindrical Pile Segment with a Soft Zone” by Xenia Karatzia, Panos Papastylianou, and George
824 Mylonakis." J. Eng. Mech., 10.1061/(ASCE)EM.1943-7889.0001001, 08215005.
825 Kulhemeyer, R.L. (1979), “Static and dynamic laterally loaded floating piles”, J. Geotech, Eng. Div.,
826 ASCE, 105, No. GT2, 289-305.
827 Muir Wood D. (2004). *Geotechnical modelling*. London: Spon Press.
828 Mylonakis, G. (1995). “Contributions to the static and seismic analysis of pile and pile-supported
829 bridge pier”, Ph.D. Dissertation, State University of New York.
830 Mylonakis, G. and Gazetas, G. (1999). “Lateral vibration and internal forces of grouped piles in
831 layered soil”. J. Geotech. Geoenviron. Eng., ASCE, 125(1), 16-25.
832 Mylonakis, G. (2001). “Elastodynamic model for large-diameter end-bearing shafts”. Soils and
833 Foundations, 41(3), 31–44.
834 Mylonakis, G. and Roumbas D. (2001). “Lateral impedance of single piles in inhomogeneous soil”.
835 4th Int. Conf. on Recent Advances in Geotech. Earthquake Eng. and Soil Dyn., San Diego.
836 Novak, M., Nogami, T. and Aboul-Ella, F. (1978). “Dynamic soil reaction for plane – strain case”, J.
837 Eng. Mech. Div., ASCE, 104(4), 953-959.
838 Pender, M. J. (1993). “Aseismic Pile Foundation Design Analysis”. Bulletin of the New Zealand
839 National Society on Earthquake Engineering, 26(1), 49-161.
840 Poulos, H.G. and Davis, E.H. (1980). *Pile foundation analysis and design*, John Willey & Sons.
841 Randolph, M.F.(1981). “The response of flexible piles to lateral loading”. Geotech., 31(2), 247-259.
842 Roesset, J.M. (1980). “Stiffness and damping coefficients of foundations”, Proc. ASCE Geotech. Eng.
843 Div. National convention, 1-30.
844 Selvadurai A. P. S., Singh B. M. and Vrbik J. (1986). *“*A Reissner-Sagoci problem for a non-
845 homogeneous elastic solid*”,* J. Elasticity, 16, 383-391.

846 Scott, R.F. (1981). *Foundation analysis*, Prentice Hall.
847 Syngros, C. (2004). Seismic response of piles and pile-supported bridge piers evaluated through case
848 histories. PhD Thesis, The City College and the Graduate Center of the City University of New York.
849 Tabesh, A., and Poulos, H. G. (2000). "A simple method for the seismic analysis of piles and its
850 comparison with the results of centrifuge tests." Proc. of 12WCEE.
851 Veletsos A. S. and Younan A. H. (1995). "Dynamic Modeling and Response of Soil – Wall
852 Systems''. J. Geotech. Eng., 120(12).
853 Vrettos, C. (1991). "Time-harmonic Boussinesq problem for a continuously non-homogeneous soil"
854 Earthquake Eng. Struct. Dyn., 20(10), 961–977.
855

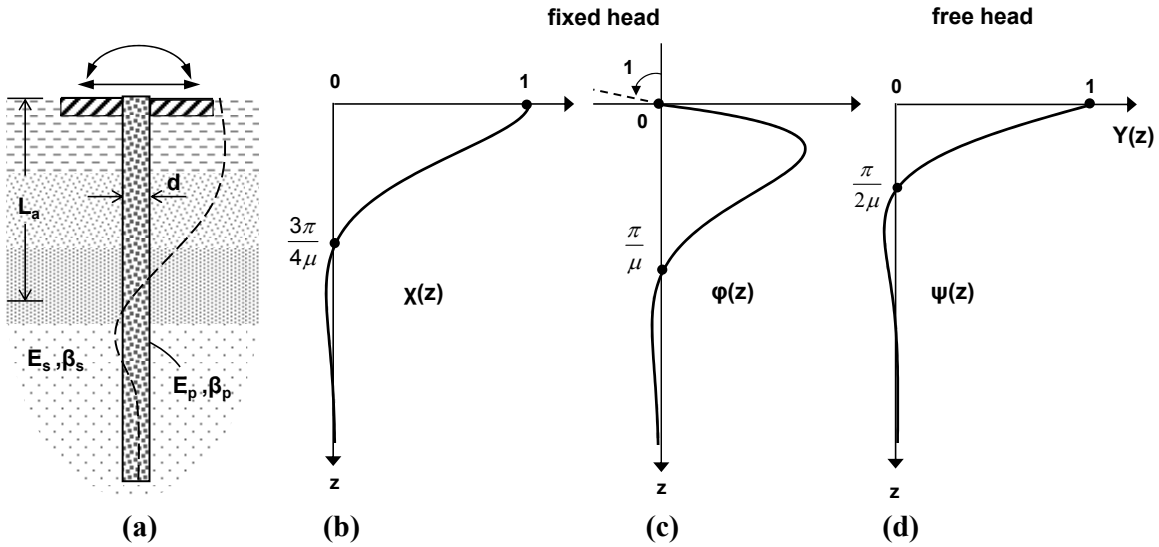

Fig. 1. a) Problem definition and active pile length, L_a; b) Unitary shape function for pile deflection due to unit head displacement under zero rotation, $\chi(z)$; c) Corresponding shape function due to unit head rotation under zero displacement, $\varphi(z)$; d) Corresponding shape function due to unit head force under zero moment, $\psi(z)$.

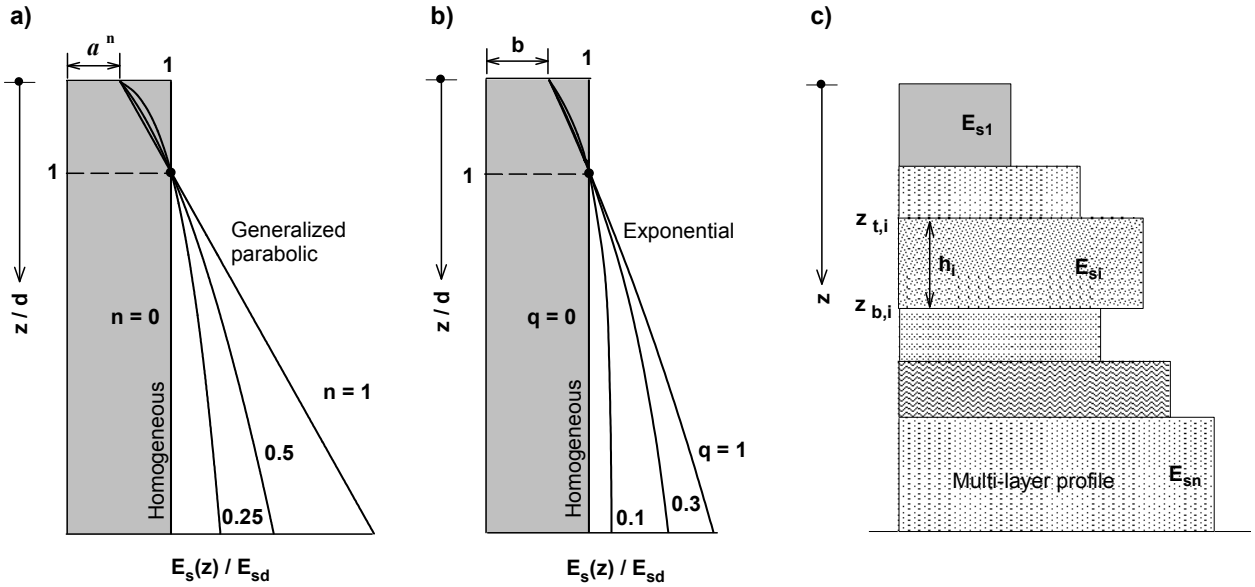

Fig. 2. Variation of soil stiffness with depth: (a) profile with unbounded parabolic increase in stiffness according to Eq. 1; (b) profile with bounded exponential increase in stiffness according to Eq. 6; (c) general multi-layer profile

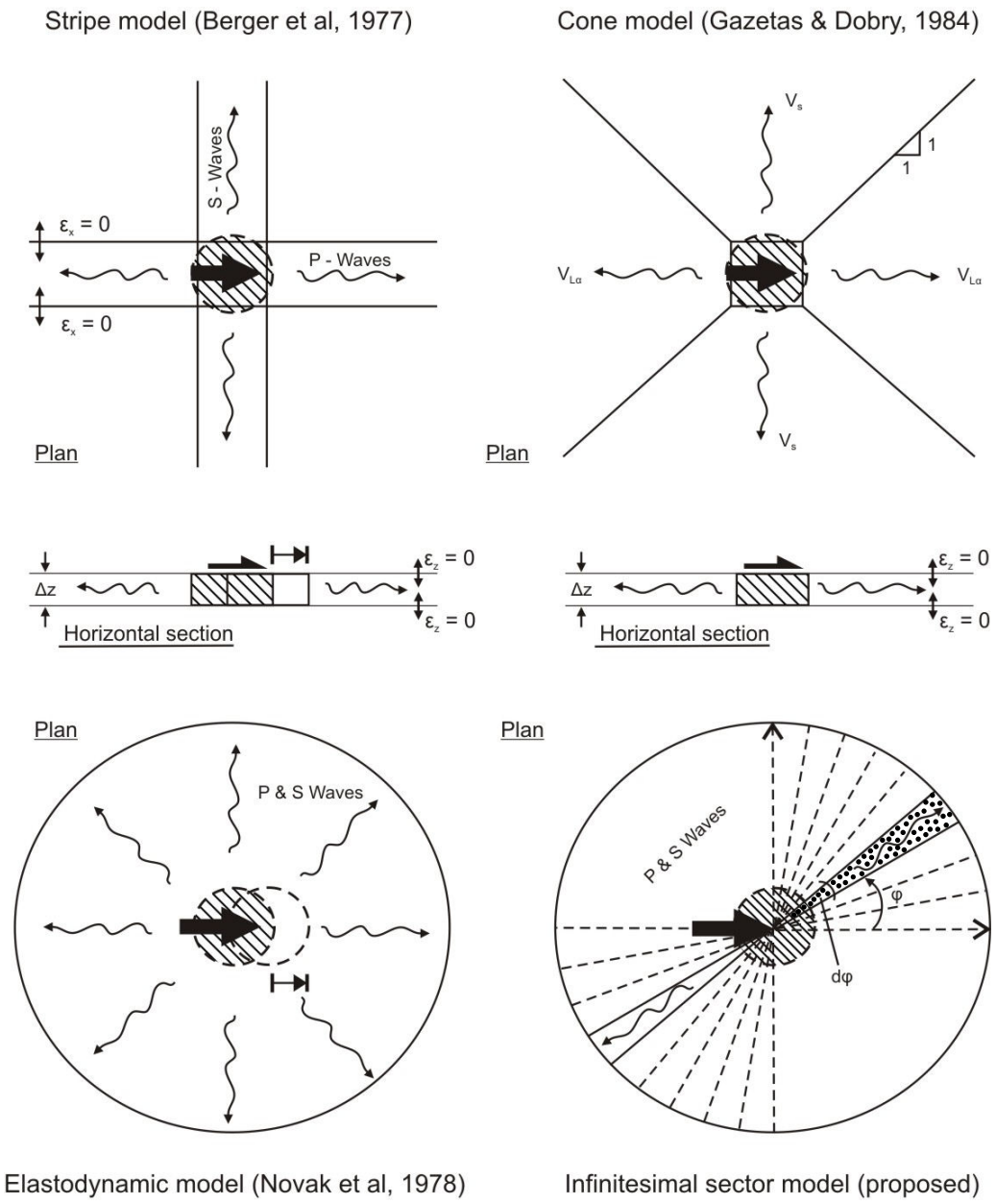

Fig. 3. Radiation damping models (modified from Gazetas & Dobry 1984).

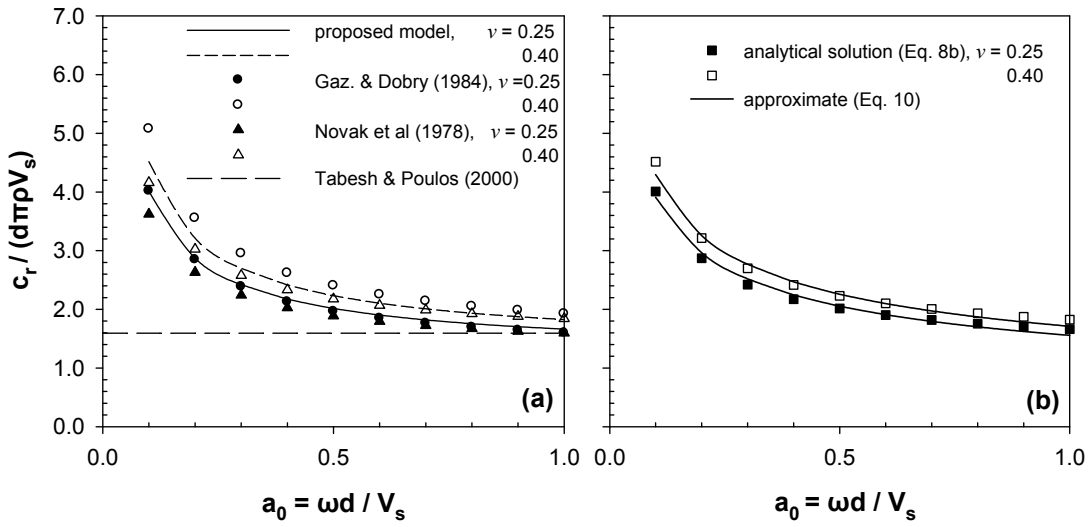

Fig. 4. Comparison of Winkler radiation dashpot coefficient obtained with the proposed model versus results from the literature, for two values of Poisson's ratio.

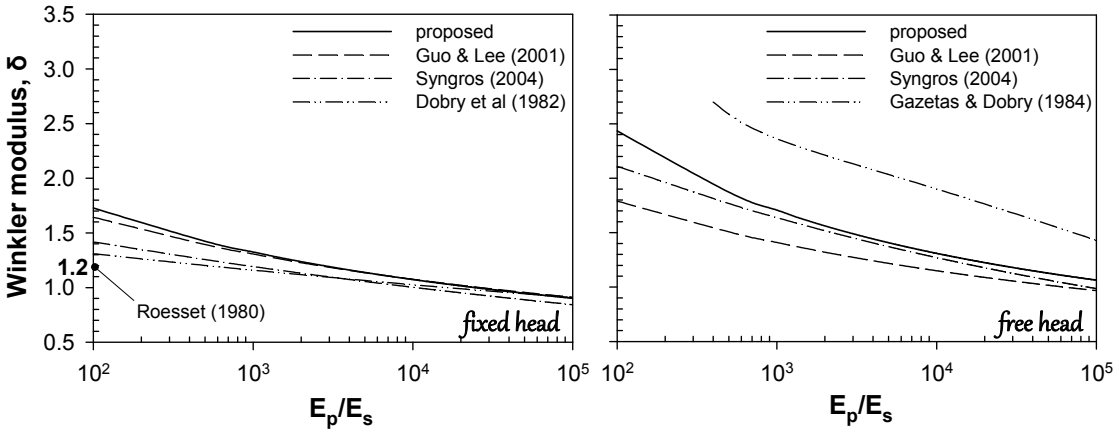

Fig. 5. Winkler modulus versus pile-soil stiffness contrast for long free- and fixed-head piles in homogeneous soil; $v = 0.4$.

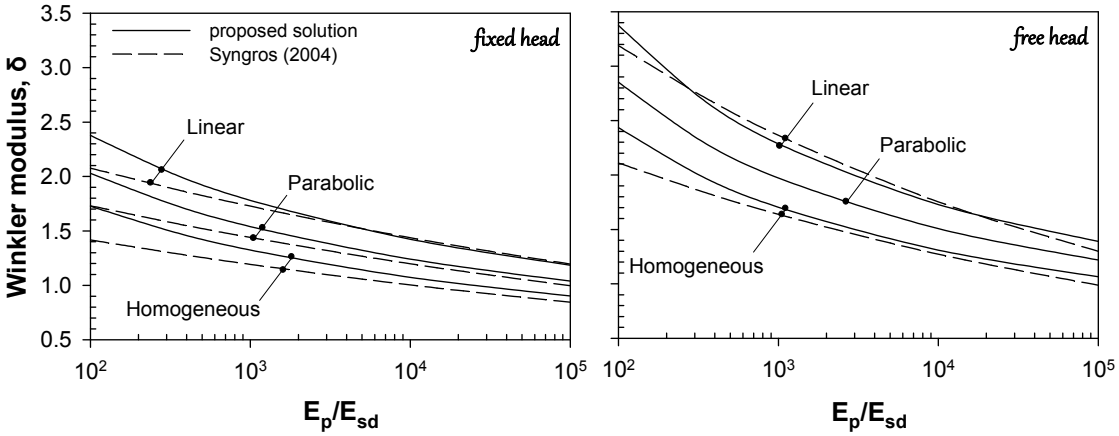

Fig. 6. Normalized Winkler modulus versus pile-soil stiffness contrast, for long fixed- and free-head piles in different soil profiles; $\nu = 0.4$.

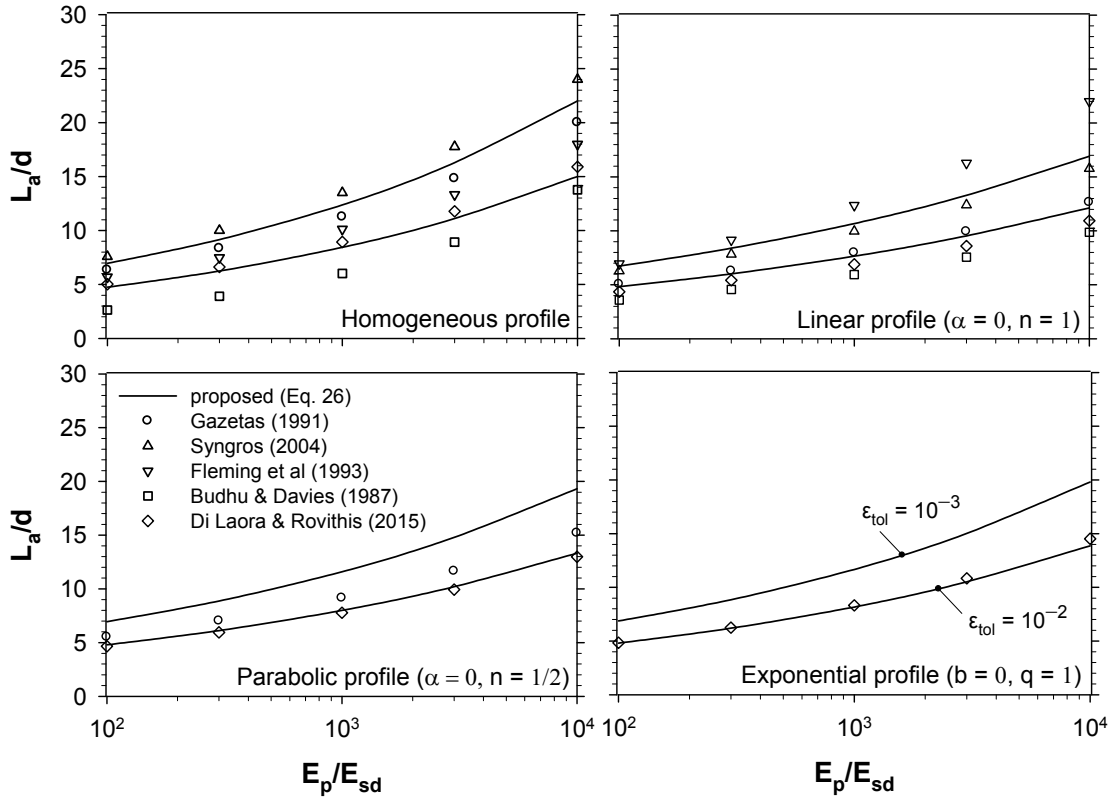

Fig. 7. Comparison of the proposed solution for active pile length L_a against results from available solutions in the literature, for various soil profiles.

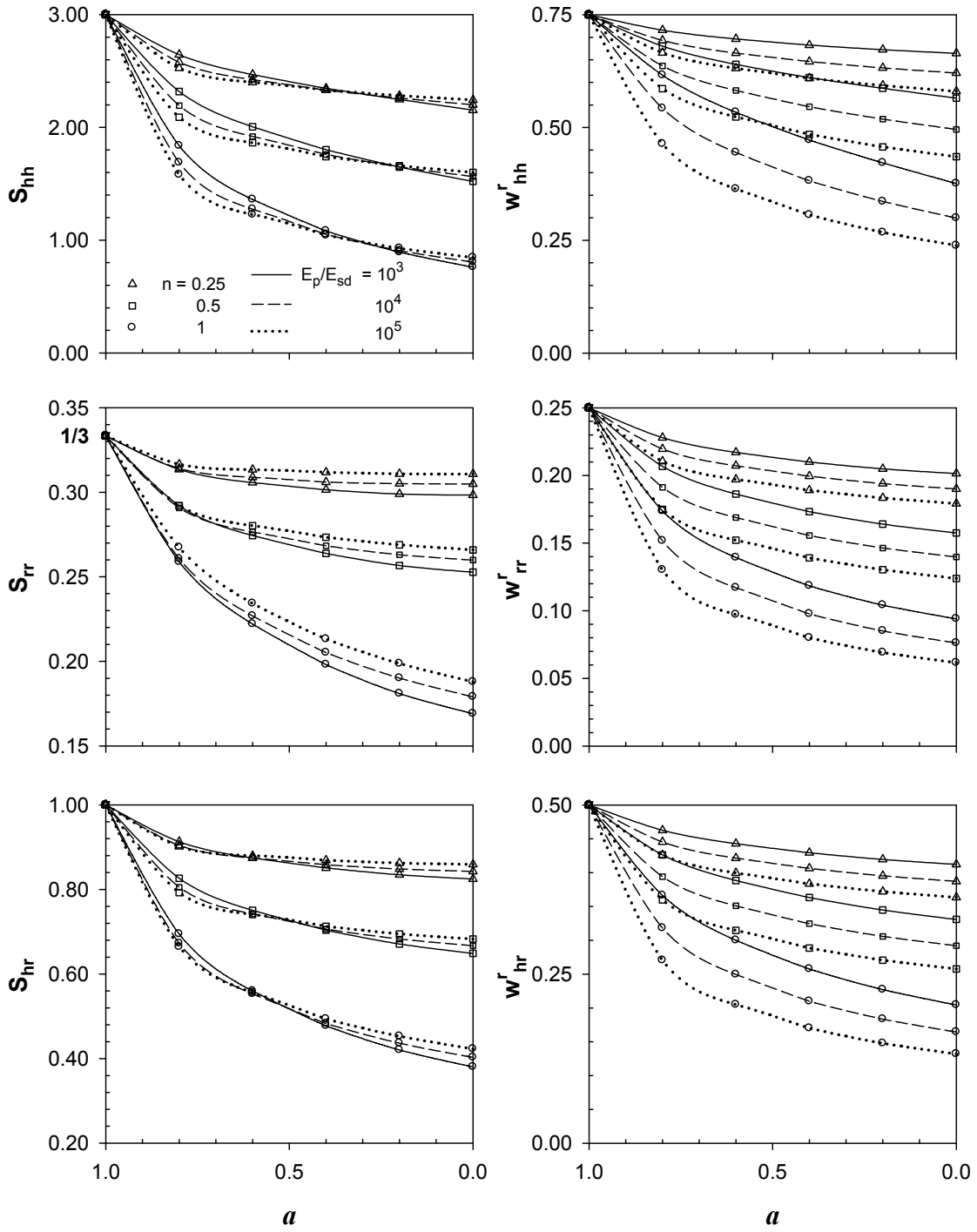

Fig. 8. Variation of coefficients S_{ij} and w^r_{ij} with inhomogeneity parameters *a*, *n* and soil-pile stiffness contrast E_p/E_{sd}, for a generalized parabolic profile.

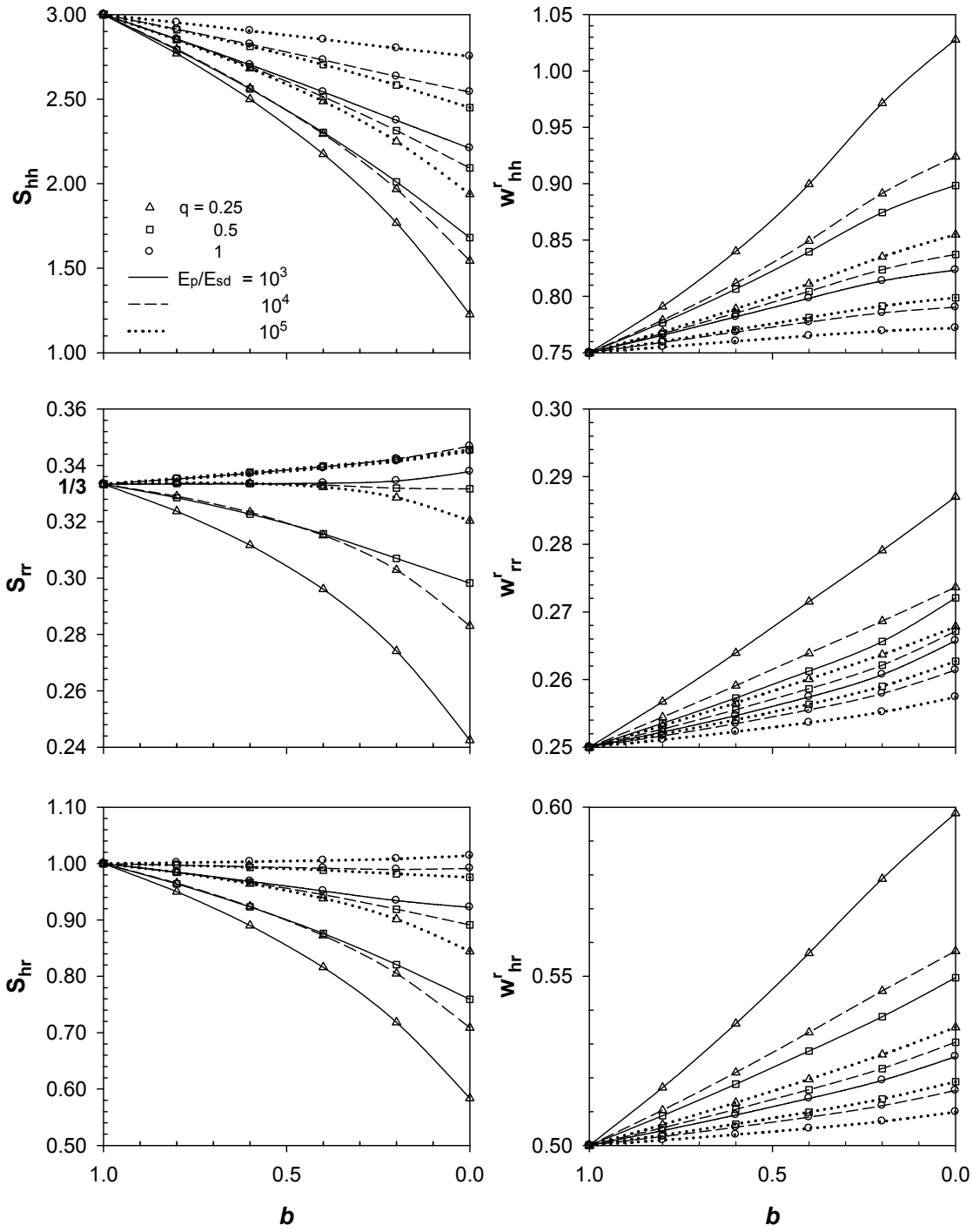

Fig. 9. Variation of coefficients S_{ij} and w^r_{ij} with inhomogeneity parameters q, b and soil-pile stiffness contrast E_p/E_{sd}, for a generalized exponential profile.

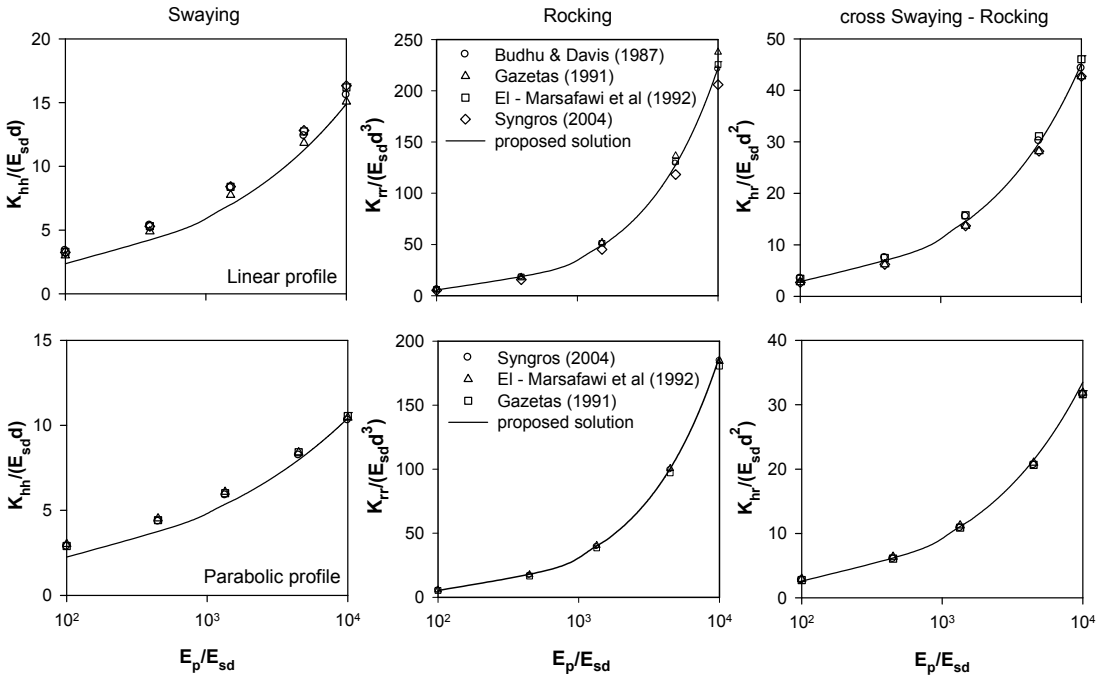

Fig. 10. Comparison of predictions from the proposed analysis against available solutions.

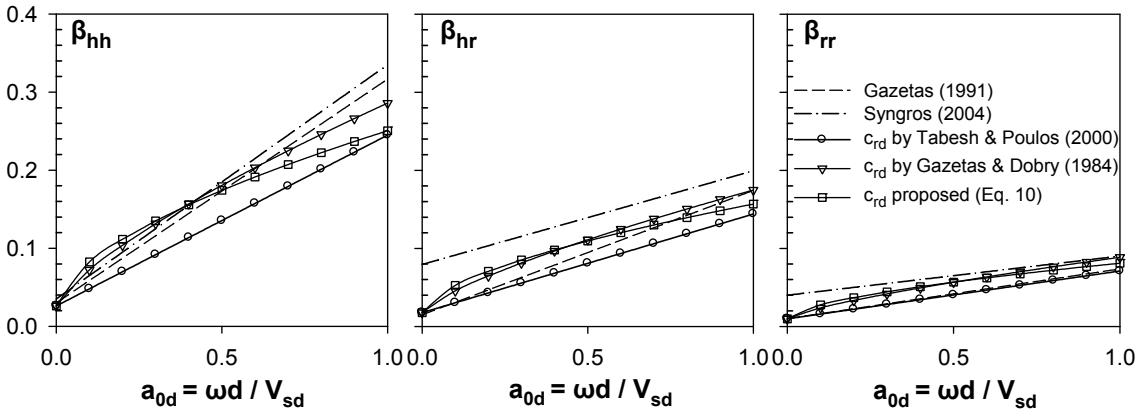

Fig. 11. Comparison of results from the proposed analysis against corresponding results from the literature for linear variation of Young's modulus with depth starting from a zero value at the top; $n = 1$, $a = 0$, $\nu = 0.4$, $\beta_s = 0.05$.

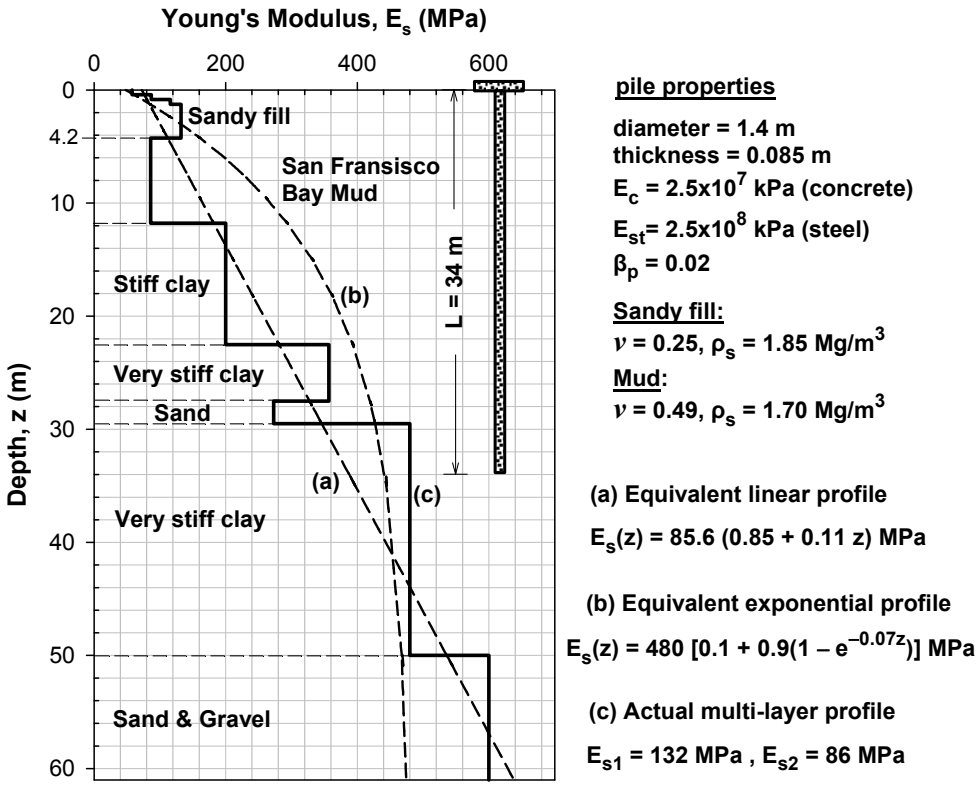

Fig. 12. Actual multi-layer soil profile, the assumed idealized linear and exponential soil profile (adopted by Gazetas & Dobry 1984)

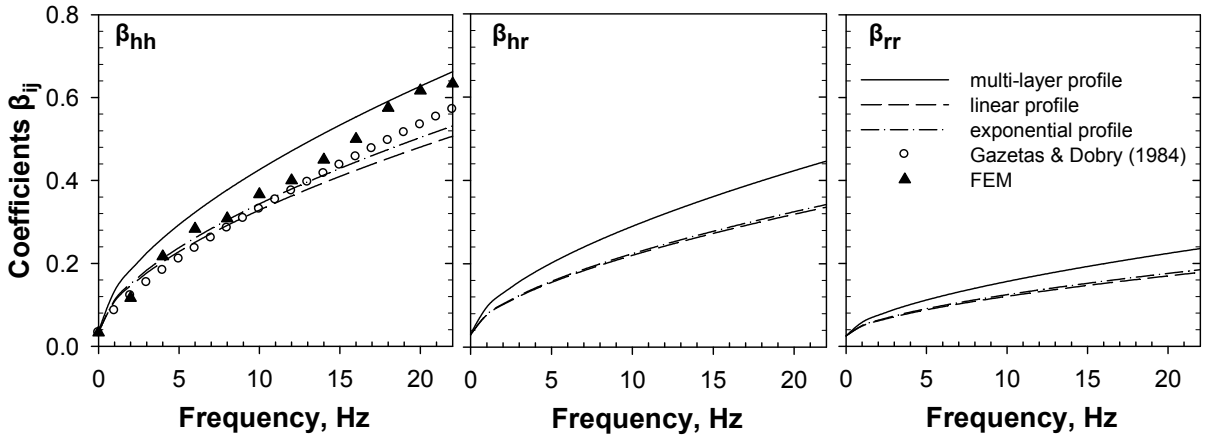

Fig. 13. Predictions for the damping coefficients β_{ij} using the actual soil profile, an equivalent idealized linear profile and a corresponding exponential profile; β_p = 0.02.

Table 1. Parameters for Winkler stiffness parameter α_c in various soil profiles

Soil profile	χ_δ				n_δ
	Fixed head		*Free head*		
Homogeneous	$\sqrt{(8/3)}\pi^{-0.25}$	(1.227)	$\sqrt{8}\pi^{-0.25}$	(2.125)	–0.250
Exponential	–	1.340	–	2.265	–0.230
Parabolic	−	1.428	−	2.272	–0.222
Linear	$\sqrt{(8/3)}$	(1.633)	$\sqrt{6}$	(2.449)	–0.200

Table 2. Parameters for active pile length in various soil profiles

Soil profile	χ_1	χ_2	χ_L		n_L
			$\varepsilon_{tol} = 10^{-2}$	$\varepsilon_{tol} = 10^{-3}$	
Homogeneous	0.100	0.700	1.50	2.20	0.250
Exponential	0.239	0.714	1.67	2.38	0.230
Parabolic	0.172	0.776	1.72	2.50	0.222
Linear	0.406	0.758	1.92	2.68	0.200